

The UV Perspective of Low-Mass Star Formation

P. C. Schneider^{1,†*} , H. M. Günther² , K. France³ ¹ Hamburger Sternwarte; astro@pcschneider.eu² Massachusetts Institute of Technology, Kavli Institute for Astrophysics and Space Research³ Department of Astrophysical and Planetary Sciences Laboratory for Atmospheric and Space Physics, University of Colorado

* Correspondence: astro@pcschneider.eu (P. C. S.)

† Current address: Hamburger Sternwarte, Gojenbergsweg 112, 21029 Hamburg, Germany

Received: date; Accepted: date; Published: date

Abstract: The formation of low-mass ($M_* \lesssim 2 M_\odot$) stars in molecular clouds involves accretion disks and jets, which are of broad astrophysical interest. Accreting stars represent the closest examples of these phenomena. Star and planet formation are also intimately connected, setting the starting point for planetary systems like our own. The ultraviolet (UV) spectral range is particularly suited to study star formation, because virtually all relevant processes radiate at temperatures associated with UV emission processes or have strong observational signatures in the UV. In this review, we describe how UV observations provide unique diagnostics for the accretion process, the physical properties of the protoplanetary disk, and jets and outflows.

Keywords: star formation, ultraviolet, low-mass stars

1. Introduction

Stars form in molecular clouds. When these clouds fragment, localized cloud regions collapse into groups of protostars. Stars with final masses between $0.08 M_\odot$ and $2 M_\odot$, broadly the progenitors of Sun-like stars, start as cores deeply embedded in a dusty envelope, where they can be seen only in the sub-mm and far-IR spectral window (so-called class 0 sources). The collapse into a central condensation is not spherically symmetric due to angular momentum conservation. Instead, an accretion disk forms while the remaining envelope still hides the inner core from view in all but the mid/far-IR (class I sources). These young objects also typically drive powerful jets that propagate through the envelope, pierce the cloud, and are often the earliest signs of a forming star. After some time, the envelope dissipates and the stars become visible in the optical. This marks the transition to class II sources, also called classical T Tauri stars (CTTSs). The period of time between disk formation and the end of the CTTS phase is highly interesting as it is the time when planet formation is thought to take place. Afterwards, the circumstellar disk disperses, planet formation halts, and accretion ceases, typically within a few Myrs. Stars in this stage are called class III sources or weak-line T Tauri stars (WTTSs). They move along Hayashi tracks towards the main sequence where they will stay most of their lifetime. If we want to understand star and planet formation, including the Sun and the solar system, “we must unravel all the mysteries of [CTTSs]” [1]. Of the different evolutionary steps, the CTTS stage is the earliest evolutionary step where UV observations can provide detailed information about the physical conditions in the disk, mass accretion onto the forming protostar, and outflow activity central to the star-formation process.

1.1. A Short History of CTTs

CTTs were initially identified as a new class of objects due their optical variability. Very early on, it was realized that they also show signs of enhanced chromospheric activity, i.e., “emission lines resembling those of the solar chromosphere” [2]. These emission lines are superposed on a photospheric spectrum similar to main sequence stars of late spectral type. Initially, the source of emission in excess of a normal photosphere was speculated to be circumstellar or chromospheric in origin [3].

The discovery that CTTs are above and to the right of the main sequence in an HR-diagram demonstrated in conjunction with theoretical work [4], that these objects must be young and, thus, the progenitors of the large main sequence population [5,6]. This notion is corroborated by the presence of strong Li absorption, which requires $\sim 100\times$ the Li abundance of the Sun [e.g. 7]. Because Li is depleted quickly in stellar interiors, the amount of surface lithium decreases with time in convective stars. Therefore, strong Li absorption can only be found in young stars and thus CTTs must be young [e.g. review by 8].

Meanwhile the number of peculiarities found in CTTs grew, but their established youth alone was insufficient to explain those peculiarities and the “mysteries” of CTTs remained. Many features, like the origin of the “chromospheric emission” remained unexplained, until the early 1980s when a large variety of models were proposed to explain features of CTTs including envelopes, outflows, infall, and dust disks.

Specifically, the “ultraviolet excess” (measured around 3700 Å) and the “blue continuum”, which go along with a weakening of photospheric absorption lines due to veiling [9,10], were shown to correlate with the strength of H α [11,12]. Such a correlation indicates a common origin of both features as observed for chromospheric emission on the Sun. Thus, it was natural to ascribe the excess continuum emission at short wavelengths to a Balmer continuum, i.e., emission following the capture of a free electron by an ionized hydrogen atom. While that finding pinpoints neither the physical origin nor location of the emitting material, it paved the way for explanations involving a suitably tuned chromosphere for producing the observed (Balmer & Ca II H+K) line fluxes in CTTs. Quantitative models of deep lying chromospheres by Cram [13] using ad hoc temperature profiles, so-called deep chromosphere models, were able to reproduce the fluxes except for H α .

These static chromospheric models, however, had difficulties in explaining the kinematic line profiles observed in CTTs [14] and additional emitting regions were required [15,16] to explain the suite of line properties and overall flux characteristic. In fact, the existence of infalling or outflowing material was already postulated by Walker [17] in 1963. The emission lines observed in CTTs often show P Cygni profiles that were initially interpreted in terms of a hot ($\sim 10^4$ K) outflow [18]—somewhat contradictory to the general infall during the cloud contraction phase [19]. Interestingly, the mass-loss rates that go along with this shell expanding at around 300 km s $^{-1}$ were estimated to a few times $10^{-8} M_{\odot}$ yr $^{-1}$, similar to modern day mass loss estimates (though not in the form of a spherical mass-loss).

The outflow explanation, however, was not entirely satisfactory, although the presence of P Cygni profiles was thought to conclusively demonstrate the existence of mass-loss in CTTs. Notwithstanding the question why CTTs should be surrounded by a shell of hot gas, the inverse P Cygni profiles expected for mass-infall are mainly seen in YY Ori stars, a class of objects that share many similarities with CTTs. The notion that mass accretion onto the central star also plays a key role in CTTs was proposed when it was discovered that the line profiles can cycle between the inverse P Cygni profile of “typical” CTTs and the inverse P Cygni profile of YY Ori objects within a few days [10,20] and it was suggested that a flattened disk, by analogy with the solar system, exists around CTTs. In fact, the IR excess of CTTs was soon to be found with the advent of IR instruments and correctly ascribed to relatively cold ($T \sim 700$ K) dust; the alternative of an optically thin gaseous envelope would produce booming Balmer continuum emission that is not observed [21]. This dust, or rather the flared protoplanetary disk around the star, is of

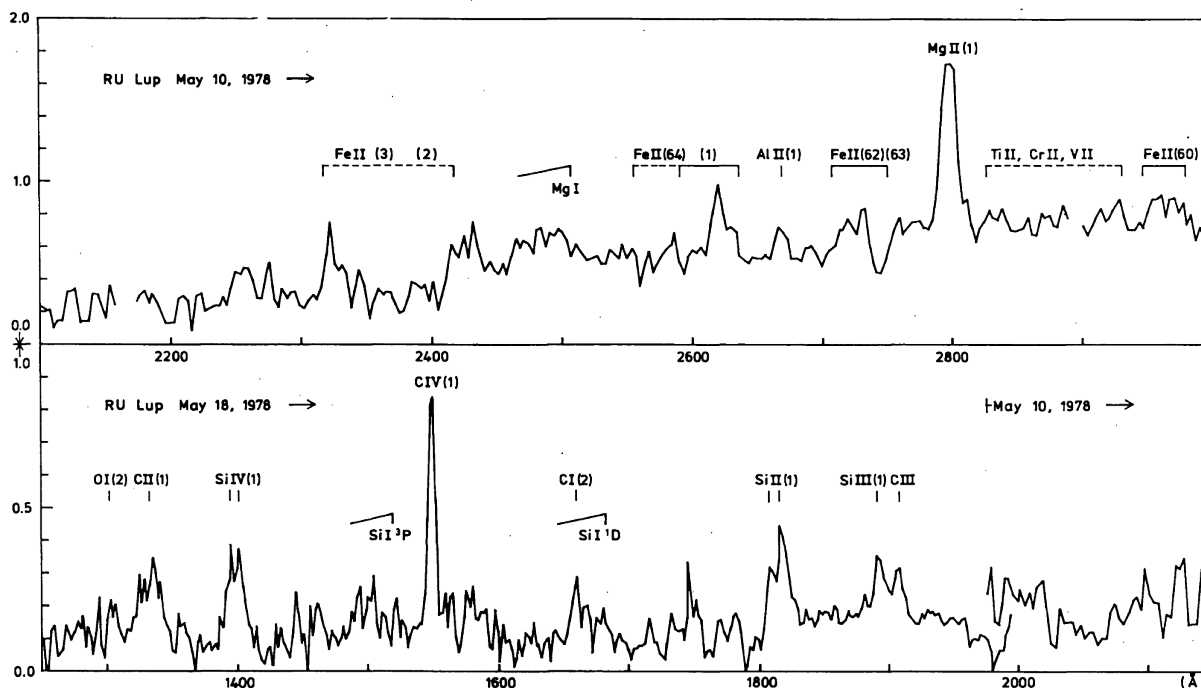


Figure 1. IUE spectrum of RU Lup (flux unit: $10^{-13} \text{ erg cm}^{-2} \text{ s}^{-1} \text{ \AA}^{-1}$) with the main features labeled, one of the first high-fidelity FUV spectra of a CTTS. From Gahm *et al.* [38]. Reproduced with permission © ESO.

exceptional importance for the study of CTTSs. In this article, however, we treat the disk just as a reservoir of material close to the central star and refer the interested reader to recent reviews for more details on protoplanetary disks [22,23].

The disk hypothesis has the great property of leaving a large fraction of the stellar photosphere with its absorption lines visible, provided that the “ultraviolet excess” emission is roughly comparable in luminosity. Walker [20] postulated a shock forming at the interface between material falling onto the star and the stellar photosphere as the source of the continuum emission and the disk as the source of the Balmer line emission—the first mention of the CTTS accretion paradigm, which is still largely accepted. Notably, it is still believed that the Balmer lines do not originate in the same region as the continuum emission although the disk itself is not considered the dominant emission region anymore. The disk accretion scenario was subsequently put on solid theoretical grounds by Lynden-Bell and Pringle [24] and Shakura and Sunyaev [25]. The accretion scenario was then specifically applied to CTTSs for explaining the line profiles including blue-shifted absorption [26]. Ulrich [26] already noted that soft X-ray emission from the post-shock plasma is expected.

1.2. The First FUV Observations of Young, Accreting Stars

With protoplanetary disks, accretion, and outflows in the form of winds and jets recognized as significant processes for CTTSs, essentially all major features of CTTS systems were identified [27] and required observational support/constraints with the “... ultraviolet spectral region [holding] promise in helping to resolve many of the issues connected with the T Tauri stars.” [28]. This statement still holds as demonstrated, e.g., by the inception of a Hubble Ultraviolet Legacy program using HST Director’s

Discretionary time, the “UV Legacy Library of Young Stars as Essential Standards” (ULLYSES) survey, which is anticipated to dedicate ~ 500 HST orbits to study low-mass star formation in the ultraviolet.

Three features make the UV spectral range particularly interesting to study CTTs: (a) Emission from hot plasma related to the accretion shock should emit most of its energy in the FUV range (already mentioned in [29]), (b) disk features seen as fluorescently excited H_2 and CO emission [30,31] and in absorption against the star [32], and (c) bright atomic emission lines from the hot post-shock region of protostellar jets and fluorescent emission from wide-angle outflows [33].

<https://www.overleaf.com/project/5e42c54e77c525000110cf18>

The first FUV (1550, 1800 Å) to NUV (2200, 2500, 3300 Å) photometric data of CTTs were obtained by the ultraviolet experiment onboard the Astronomical Netherlands Satellite (ANS, [34]). Targeting seven of the “most prominent” CTTs, three were detected [35]. In the discovery paper, de Boer [35] specifically discuss the FUV properties of V 380 Ori, which showed excess emission that they associate with the Balmer continuum produced by dense gas. Interestingly, these authors already state that dereddening FUV fluxes of CTTs is subject to comparably large uncertainties, still one of the unsolved uncertainties when studying CTTs (see discussion in France *et al.* [36]).

A big step forward for FUV studies of CTTs was the launch of the IUE satellite [37], which provided the opportunity to measure individual lines in larger samples of CTTs. Figure 1 shows an IUE spectrum of the CTTs RU Lup [38], still representative for most CTTs FUV spectra. The spectrum is dominated by strong emission lines from ionized species with the presence of C IV, Si IV, and Mg II and Gahm *et al.* [38] suggested regions with $\log T \approx 4.5 - 5.0$ “around” the star, a notion that essentially holds today as most of the hot lines are thought to arise from material somehow influenced by accretion.

Figure 2 provides a sketch of the most relevant FUV emission regions in CTTs. In the next sections, we successively describe how FUV studies continue to provide key information for the physical processes in CTTs. We begin with the intrinsic FUV emission of the star due to enhanced magnetic activity, move then successively outwards, i.e., we then discuss the emission thought to arise from accretion, the disk features, and emission from outflows and jets. We close with a quick prospectus on future UV disk studies.

2. Stellar UV emission of CTTs from magnetic activity

Young stars are rapid rotators with typical rotation periods of a few days [39–42], because the stars retain some of the angular momentum from their natal cloud during the contraction phase. In addition, T Tauri stars possess largely convective interiors while moving from the birth line towards the zero age main sequence (ZAMS) so that they are able to generate kiloGauss magnetic fields [43]. As a result, T Tauri stars show all signs of enhanced magnetic activity in the form of strong chromospheric and coronal emission compared to their main sequence siblings [44,45].

In non-accreting stars, chromospheric activity causes emission in excess to that expected from the stellar photosphere and particularly WTTSs are highly magnetically active [46]. This enhanced magnetic activity is due to extended outer, rarefied layers of the atmosphere with temperatures between about $T = 10^4$ and 10^7 K. Above the photosphere, one finds the chromosphere ($T \sim 10^4$) and a transition region (TR, $T \sim 10^5$ K) connecting the chromosphere with the corona ($T \sim 10^{6-7}$ K). As a rule of thumb, chromospheric and TR emission is most prominent in the UV range while the corona emits mostly in the X-ray regime.

For the study of genuine star formation related processes, e.g., accretion, the enhanced magnetic activity of T Tauri stars is a nuisance, because the chromospheric and TR emission from magnetic activity must be carefully separated/subtracted. WTTSs are excellent templates for the emission caused by magnetic activity, because they lack accretion and gas-rich disks, but share internal structure and rotation with the CTTs. Using a magnetically inactive dwarf as a template for the UV emission instead of

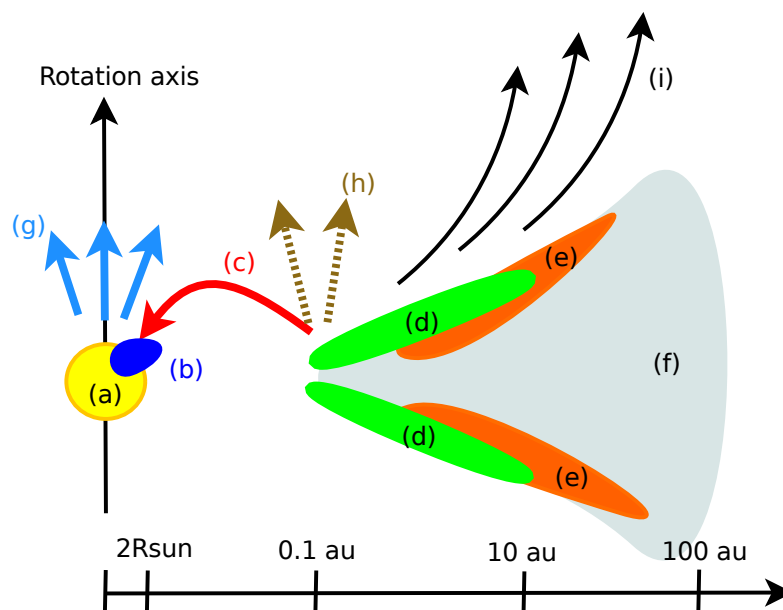


Figure 2. Sketch of a CTTS system with regions that are relevant for FUV studies labeled. Relative positions are correct, but relative distances and sizes are not. The relevant components are (a) the pre-main sequence star, (b) the accretion shock on the stellar surface, (c) the accretion funnel, (d) the inner, hot disk region, ($T \sim 2,000$ K) (e) cooler regions of the inner disk surface ($T \sim 500$ K), (f) cool protoplanetary disk material, (g) a spherical (stellar) wind, which may be seen in emission or as an absorption component in strong emission lines (e.g., C IV), (h) an X-wind, (i) a disk wind.

a WTTS may result in the erroneous conclusion that a particular star is accreting at a significant rate ($\dot{M} \sim 10^{-8.5} M_{\odot} \text{ yr}^{-1}$, [47]).

It is therefore not surprising that many large observing programs studying CTTSs included a number of WTTSs as templates to distinguish emission from magnetic activity and, e.g., accretion [48, and Fig. 3]. Any emission in excess of the chromospheric to coronal flux of WTTSs is, as a starting hypothesis, thought to be attributable to star formation processes such as accretion, disks, or jets. (In fact, no theory exists that covers self-consistently all FUV emission components of CTTSs.) Therefore, we define the term “excess emission” in the context of this article as the emission not seen in a comparable WTTSs although we note that WTTSs show some spread in their UV properties [49].

3. Accretion

CTTSs possess strong stellar magnetic fields in the kG range [50], compared to just a few G average surface fields on solar mass main-sequence stars. The strong magnetic fields truncate the disk at a few stellar radii so that accretion proceeds along magnetic field lines connecting the star and the inner disk [51]. This leads to a strong shock, where the infalling material impacts the stellar atmosphere (see Fig. 2). Since typical free-fall velocities are around 300 km s^{-1} , the post shock temperature is in the MK range and

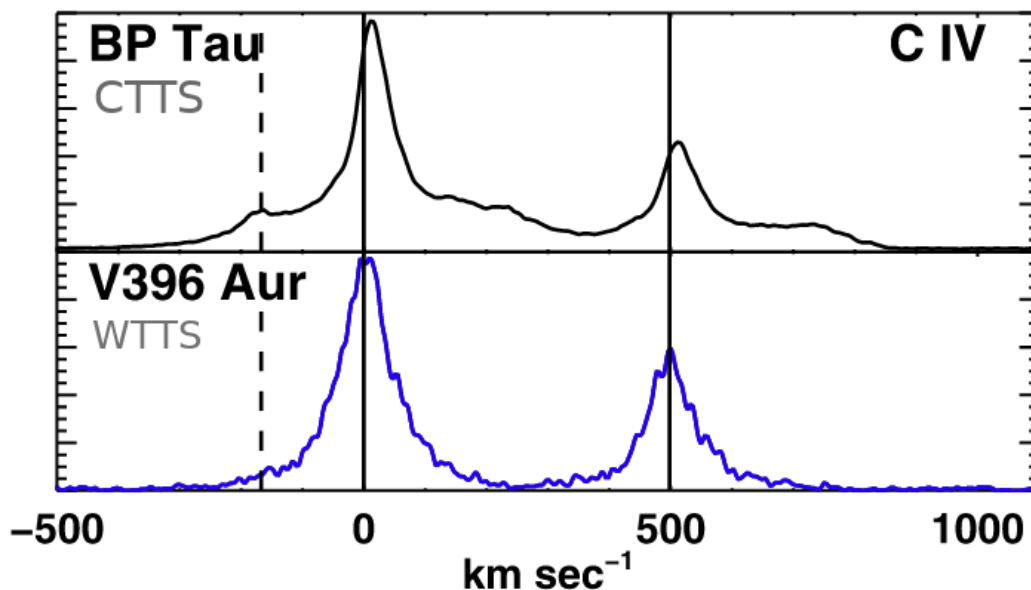


Figure 3. Comparison of a typical CTTSs line profile (top), here C IV, and that of a comparable mass WTTs (bottom). The dashed line marks the location of emission from fluorescent H₂. From Ardila *et al.* [64]. ©AAS. Reproduced with permission.

the plasma cools predominately through X-ray emission, which is then partly reprocessed into UV and optical radiation [52,53]. The accretion hot spot covers on the order of 1 % of the stellar surface, so that the densities in the accretion funnel should be around 10^{12} cm^{-3} to provide the accretion rates in the observed $10^{-8} M_{\odot} \text{ yr}^{-1}$ range [52]. This accretion-driven high-energy emission represents the main ionizing agent at the surface of the protoplanetary disk, where the material is transported inwards [54]. There is general consensus that the main features of this picture are correct, but key processes remain uncertain—especially when it comes to attributing FUV emission to individual processes.

At FUV wavelengths, the main diagnostics of accretion are enhanced fluxes in hot ion lines like C IV (Fig. 3). Three properties demonstrate that accretion indeed is the root cause of the excess in these lines:

1. Monitoring campaigns of individual objects such as BP Tau show that the FUV fluxes vary in conjunction with optical excess emission [55–57].
2. Line fluxes exceed those of WTTs and other magnetically active stars [58]; still, the luminosity in, e.g., C IV is only a tiny fraction ($\sim 0.1\%$) of the accretion luminosity [59].
3. The lines are broader in CTTSs than in WTTs [60].

In particular Johns-Krull *et al.* [58] find that the “emission line luminosity in the high ionization lines present ... correlates well with the mass accretion rate.”. However, these authors also noted that the existence of the correlation depends critically on the source of their extinction values. A significant correlation results only for a certain set of extinction values and this strong dependence on the often uncertain UV extinction is still relevant today.

Later, the relation between FUV fluxes in hot ion lines and accretion was confirmed by Yang *et al.* [see Fig. 5, 61] with a large set of 91 stars with data from HST ACS, STIS, and GHRS lending further support to the notion that accretion is indeed responsible for the bright emission in hot ion lines. Interestingly, the ratio between fractional line luminosities of different ions, e.g., C IV and O I $\lambda 1304$, is the same in CTTSs as in WTTs although the respective peak line formation temperatures are very different ($\log T \sim 4$ vs

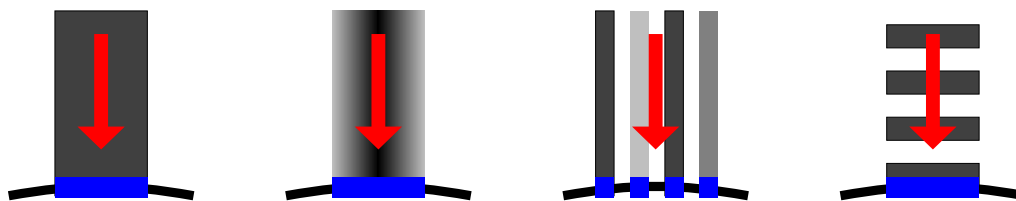


Figure 4. Some scenarios for the structure of accretion columns. The stellar surface is at the bottom and material flows along a magnetic field line onto the stellar surface (indicated by the red arrow). The accretion shock (blue) forms on the stellar surface. Density is shown as gray scale. From left to right: (1) One homogeneous column with one density and a single infall velocity; (2) one column with a density stratification (high density in the center of the column indicated by the black region, lower density in outer region indicated by the grayish color) and one infall velocity; (3) multiple columns that are individually homogeneous, i.e., have different densities but are otherwise equal; (4) one “column” is decomposed into individual blobs that are, individually, homogeneous in density.

5) and although CTTS line fluxes are one to two orders of magnitudes higher than those of comparable WTTSs [cf. Fig. 5 right and 61].

Pinpointing the origin of the hot ion lines is challenging and currently an open issue; different scenarios for the accretion column have been proposed (cf. Fig. 4). Most of the accretion funnel has only $T \sim 10,000$ K [62,63], therefore only two regions may generate the accretion contribution to the hot ion emission. The material of the funnel immediately above the shock (the radiative precursor) or postshock material are the only likely sources of the hot ion line excess [64].

The relative importance of pre- and post-shock regions depends mainly on shock velocity and density [65]. Both components should have red-shifted velocities: Material in the funnel should have velocities of a few 100 km s^{-1} while the shocked material will be at velocities of just tens of km s^{-1} and the expected line profile is rather narrow (e.g., for the typical $v_{in} = 300 \text{ km s}^{-1}$, $v_{post} = 70 \text{ km s}^{-1}$). However, in the Goddard High Resolution Spectrograph (GHRS) spectra ($R \sim 20,000$) of eight CTTS presented by Ardila *et al.* [66], one finds broad emission lines from hot ions (C IV, Si IV, etc.) with a range of centroid velocities (from blue-shifted to centrally peaked to red-shifted). Also higher excitation lines like O VI show a great variety of line profiles, again including peaks that are blue- and red-shifted from the stellar rest velocity [67]. Later studies using STIS [68] as well as COS data [64] confirm these trends revealing sometimes complex line profiles that may be modified through absorption or emission by outflowing material. When the Si IV line profile can be measured under the H₂ emission, the C IV line shapes agree relatively well. However, the line ratios between the blue and red members of the doublets agree with the ratio expected from optical thin emission only (generally) for C IV and not for Si IV, which is puzzling given that the radiative precursor should be optically thin to both, Si IV and C IV [65] (although this implicitly assumes that the lines are predominately collisionally excited). Furthermore, the C IV line shape agrees with that of Si III], which is thought to come from the radiative precursor [69].

In a comprehensive analysis of FUV lines from CTTSSs using HST COS data, Ardila *et al.* [64] demonstrate that most hot ion lines, in particular Si IV, C IV, and N V, share one kinematic profile and can be decomposed into a narrow and broad component. The ratio between these two components depends on the accretion with the narrow component’s contribution increasing with accretion rate.

It is interesting to note that the conversion from FUV line fluxes to stellar accretion rate is based on empirical correlations between the FUV line fluxes and other, perhaps more traditional, accretion tracers like H α equivalent width (EW) or veiling measurements [58]. Application of the Calvet and Gullbring [52] shock models by Ingleby *et al.* [70] to the NUV to optical spectrum of CTTSSs revealed

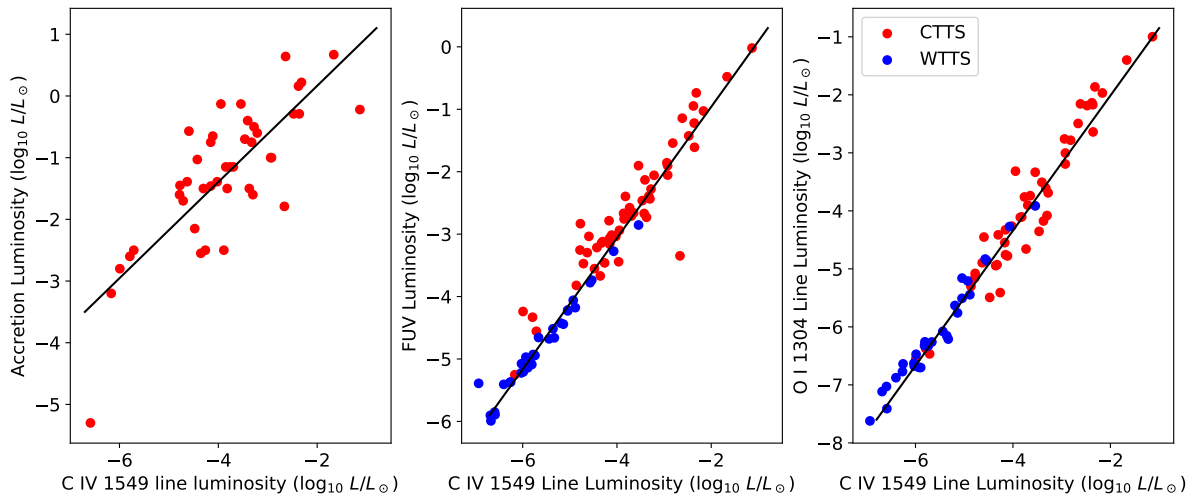


Figure 5. **Left:** Correlation between extinction corrected C IV and accretion luminosity. This suggests that the C IV in CTTSs is mostly due to the accretion process. **Middle:** Correlation between C IV and total UV luminosity. **Right:** Relation between line fluxes. Data and fits from Yang *et al.* [61].

that the same accretion column (specified by their energy flux) cannot simultaneously reproduce the UV and optical ranges of the spectrum; these authors require the existence of multiple accretion columns with different F-values, i.e., different densities for the same infall velocity. With this prescription, the emission of the different funnels peaks at different wavelengths and a more precise (but not necessarily accurate) description of the excess flux is achieved, which also modifies the derived accretion rate by roughly a factor of two ([70], [71]). Such a scenario (multiple accretion columns with different densities) is appealing, because it may explain (a) that UV line ratios indicate rather low densities in the emitting region (10^{10} cm^{-3}) based on ratios between the He II and C IV lines [64] as well as semi-forbidden lines that should be optically thin [72]. In addition, (b), this could explain the varying ratio between the narrow and broad components, because part of the post-shock material may be buried in the photosphere and a varying ratio of the pre- and post-shock plasma is seen depending on the exact accretion geometry [64]. A detailed description of the accretion process is beyond the scope of this review, however, we think that there are not necessarily different accretion funnels, but rather one column with a density stratification (see sketch in Fig. 4) and we note that structured accretion streams may also explain some of the X-ray diagnostics [e.g. 73–75]. In this picture, the individual funnels with different densities are replaced by a single column, but with a continuum of densities so that the description of the excess emission as a sum of different density columns is just a simplification of the true column structure and the accretion column may also possess some structure along the flow direction. In summary, our picture of the accretion funnel evolved over the last two decades from a single monolithic column to a structure that is stratified in density along the radius with an additional density modulation along the infall direction. As of 2020, however, there is no quantitative model that simultaneously reproduces the optical/NUV/FUV features of accretion emission (although individual aspects can be reproduced in simulations). We need both simultaneous observations from the X-ray to the optical range as well as theoretical work to self-consistently describe the accretion process of CTTSs.

4. Protoplanetary Disks

Circumstellar accretion disks are essential components of CTTS systems. They are typically studied at infrared to mm-wavelengths as those are the wavelengths where most of the energy received from the central star is re-radiated [23]. These so-called protoplanetary disks are not only the sites of ongoing planet formation, but are also highly structured and dynamic objects with features like warps, (dust) gaps, and spirals (e.g. [76]). It is currently debated if these features can be ordered into a sequence in time; in particular, if so-called transitional disks (TDs), which harbor significant (dust) gaps, are more evolved disks compared to full gas and dust disks.

Protoplanetary disks are thought to consist mainly of gas with just about one percent of the mass in dust like the ISM. The local physical properties like temperature and density depend, to first order, mainly on radius and height within the disk (see sketch in Fig. 2). One would like to study both the disk gas and dust since gas controls its dynamics while the dust is highly relevant for the formation of planetary cores. Observationally, the dust is more readily accessible compared to the gas, because of its continuum emission at sub-mm wavelength while observing protoplanetary disk gas requires more challenging spectroscopic line measurements.

The dominant species of protoplanetary disks, molecular hydrogen, is difficult to observe directly, because the electric dipole transitions between rotational and vibrational states are forbidden as H_2 has no net dipole moment. H_2 can undergo quadrupole rotational transitions that produce weak emission lines in the mid-IR due to low oscillator strengths. The large spacing between even the lowest energy levels makes it, however, difficult to excite the molecules via collisions in cold gas of the disk midplane. Therefore, the IR- H_2 lines are weak and most sample surveys find a relatively low detection rate with accordingly tight constraints on the amount of warm ($\gtrsim 500$ K) molecular hydrogen in the disks [77,78]. Carbon monoxide (CO) is often used as a tracer for the disk's gas content, especially with the advent of ALMA. However, the interpretation of the CO emission is challenging since CO may freeze-out on dust grains and detailed models are required to convert the measured emission line fluxes into gas disk masses [79]. Therefore, complementary diagnostics of the disk's gas are highly desired.

On first sight, it may appear surprising that gas disk diagnostics reside in the FUV because equilibrium temperatures in the disk are very low (tens to hundreds of K) compared to the peak formation temperatures of prominent atomic emission lines (like C IV at $\sim 10^5$ K). Nevertheless, FUV observations of (i) fluorescently excited molecular emission lines, (ii) the 1600 Å bump, and (iii) disk absorption features provide unique information on disk chemistry and dispersal.

4.1. Fluorescently Excited Molecular Emission Lines

In contrast to the weak IR- H_2 lines, the FUV transitions of H_2 have large oscillator strengths. These lines result from electronic Lyman- and Werner-band transitions, which break symmetries in the molecular structure and enable dipole-allowed transitions. The UV- H_2 features originate from a population of vibrationally excited gas "pumped" from the ground electronic state into the low-lying excited electronic states by Ly α photons, the strongest stellar emission line in the FUV [31]. Depending on the pumping wavelength, molecular hydrogen is excited into the Lyman ($2p\sigma B^1\Sigma_u^+$, [80]) or Werner ($2p\pi C^1\Pi_u$, [81]) electronic bands. Each excited state emits a characteristic spectrum, called progression, with known ratios between the individual lines for each progression. The dipole-allowed transitions have large Einstein coefficients ($A_{ul} \sim 10^8 \text{ s}^{-1}$) so that these electronic states will decay instantaneously in a fluorescent cascade down to one of many different rovibrational levels in the ground electronic state ($X^1\Sigma_u^+$, [30]).

In protoplanetary disks, the UV- H_2 emission originates in the inner regions ($0.1 < r \lesssim 10$ au) [30,82–84] where gas temperatures can reach the 1500 K threshold required for Ly α fluorescence to take place [85]. A large number of fluorescent UV- H_2 emission lines are observed in the 1050–1700 Å wavelength

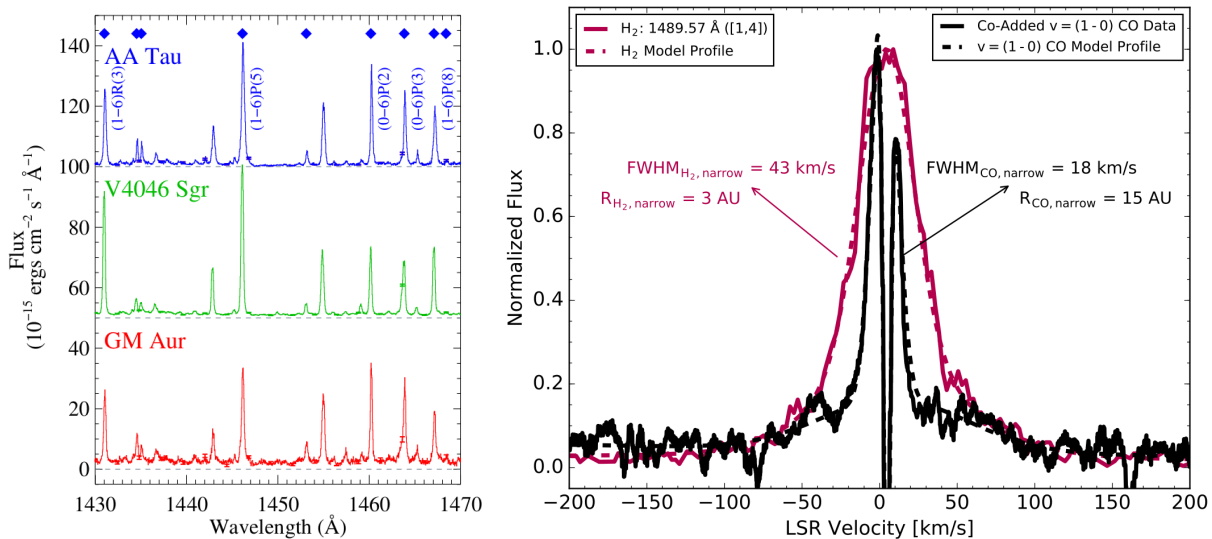


Figure 6. **Left:** 1430–1470 Å spectral region for three prototypical gas-rich disks. All of the strong spectral features in this bandpass are emission lines from Ly α -pumped fluorescent H₂ (UV-H₂; marked with blue diamonds and several bright features are labeled). From France *et al.* [83]. **Right:** Kinematic model for the H₂ emission including the effect of the COS line spread function (LSF). From Arulanantham *et al.* [118]. Both figures: ©AAS. Reproduced with permission.

range [30,83] accessible by HST observations (see Fig. 6). The UV-H₂ fluxes correlate with hot ion line fluxes like C IV, which suggests that one mechanism controls the FUV spectrum [58]—and accretion appears as the most probable candidate, because higher accretion rates imply more Ly α with a resulting higher excitation rate of the UV-H₂ lines. The existence of UV-H₂ as well as CO strongly suggest that both the CO and H₂ in the inner disk are shielded by very little neutral hydrogen [31,86].

Herczeg *et al.* [30] measured 146 UV-H₂ emission lines from TW Hya with *HST*-STIS and find that the features are coincident with the star in velocity space and not spatially extended beyond the 0.05" resolution of the instrument, as would be expected for emission from an outflow. These observations indicate that the emitting H₂ is located in the inner regions of the protoplanetary disk (within $r \sim 1.4$ AU at the distance of 56 pc to TW Hya). Nevertheless, some contribution from an outflow may be present as the H₂ line centroids are generally slightly blue-shifted [68] and do not typically show the double-peaked profiles expected from a pure disk emission model [84], see also sect. 5.

In CTTs, one observes a number of H₂ absorption features against the wings of the stellar Ly α line. The relative depths of these H₂ absorption features depend on the respective absorbing column density $N(H_2, \nu, J)$. The relative population of these states depends on the total column density and the excitation temperature (assuming a single, thermal population of absorbing molecular hydrogen [87]). Measuring numerous absorption features for 22 CTTs, Hoadley *et al.* [88] find that (a) the low energy states follow the pattern expected for $T \sim 2,000$ K while the high-energy states of H₂ show higher occupancies than expected. These authors speculate that the non-thermal populations arise in a diffuse molecular disk atmosphere where level populations are driven out of thermal equilibrium by Ly α photon pumping.

Kinematic modelling is another powerful technique to derive spatial information from the UV-H₂ emission lines as the spectral resolution of the UV instruments onboard HST is sufficient given the velocities expected in the inner disk region [84,89]. Assuming that the emission at each radius has a Keplerian profile, the radial profile of the molecular hydrogen emission can be reconstructed, see Fig. 6. The emission is confined to $r < 10$ au for most sources with a characteristic emission radius of just about 1 au, which

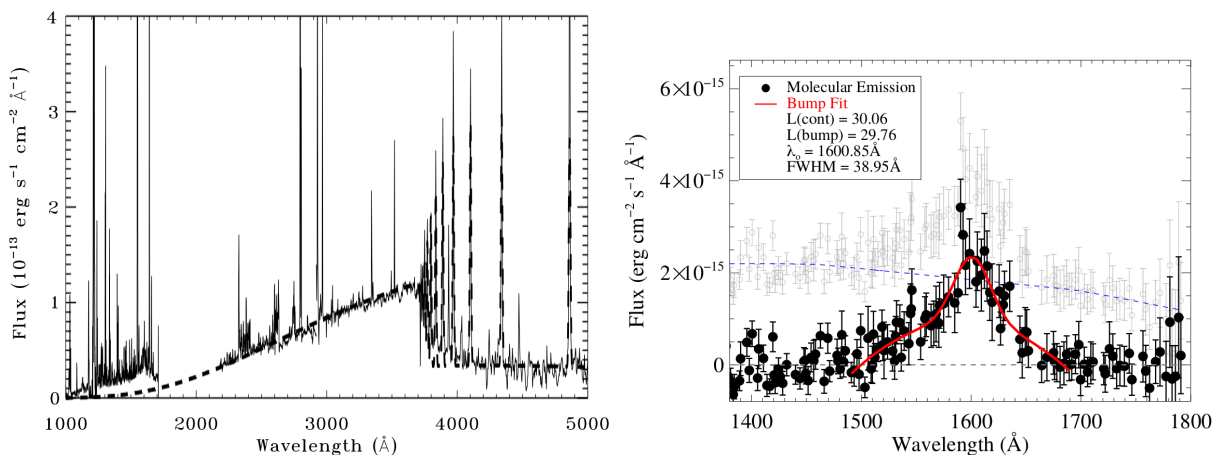


Figure 7. **Left:** FUV to optical spectrum of the nearest CTTS, TW Hya, after subtraction of WTTS template spectrum of V819 Tau. The dashed line indicates the expected emission from the accretion model, which approximates the NUV continuum of TW Hya but significantly underestimates the FUV continuum, especially around 1600 Å. From Herczeg *et al.* [82]. **Right:** Typical 1600 Å-Bump spectrum, here for CS Cha. The blue-dashed line indicates the polynomial model used to subtract the accretion continuum. From France *et al.* [36]. Both figures: ©AAS. Reproduced with permission.

agrees with the upper limits imposed by the spatial analysis of STIS data [90]. The UV-H₂ emission can be also used to study the evolution of disk gas with system age as described in more detail in sect. 4.5.

The second most abundant species in protoplanetary disks, CO, also emits in the FUV. Photo-excited CO gas traces cooler disk regions compared to H₂ (UV-CO; $T \sim 200 - 500$ K). Its emission originates from several ro-vibrational bands of the $A^1\Pi - X^1\Sigma^+$ (Fourth Positive) electronic transition system. Similar to the UV-H₂, the UV-CO emission is pumped by stellar (accretion driven) Ly α and partly by C IV photons. Schindhelm *et al.* [31] detect UV-CO emission from $T \sim 500$ K gas in roughly half of the FUV disk spectra, i.e., a different population than the warmer CO gas ($T \sim 300 - 1500$ K) well studied in the strong fundamental band rovibrational emission lines at 4.7-5 μm [91–93]. These differences may be attributed to the FUV CO population residing more distant from the star than either the IR-CO or UV-H₂ emitting gas [31]. Compared to UV-H₂, the signal of the UV-CO lines is weaker and kinematic modelling subject to larger uncertainties. Generally, however, the UV-CO emission correlates with the stellar Ly α emission, i.e., mainly with accretion rate. The second strongest parameter controlling the the UV-CO emission may be the dust and gas opacity of the inner disk, or in other words, observations of UV-CO emission is more indicative of the dispersal of cooler gas than UV-H₂ emission.

4.2. The “1600 Å Bump”

The FUV continuum emission of CTTSs is comparably weak, because both, the stellar and the accretion continuum, decline towards shorter wavelengths; in contrast, the accretion continuum is readily detected in the NUV [70]. Therefore, good continuum measurements require high S/N and the discovery of a broad (50–200 Å) emission feature, roughly centered on 1600 Å in the FUV continuum of CTTSs was somewhat surprising [see Fig. 7 and refs 82,94,95]. In fact, the dominant bump formation is still not entirely clear, but most likely results from line and continuum emission from vibrationally excited H₂.

France *et al.* [36] detect the 1600 Å-Bump in 19 out of 37 CTTSs surveyed. The detection rate is 100% in transition disks compared to about one third in primordial or non-transition disk sources. Because the integrated flux of the 1600 Å-Bump is a significant fraction of the entire H₂ and continuum flux, France *et al.*

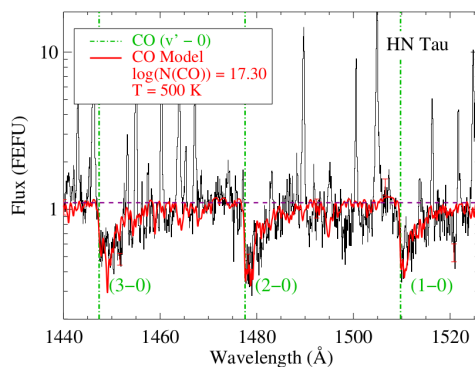


Figure 8. CO absorption in the CTTS HN Tau. Data shown in black, fit of the CO transmission spectrum in red and the green line indicates the bandheads (1 FEFU = 10^{-15} ergs $\text{cm}^{-2} \text{s}^{-1} \text{Å}^{-1}$). From France *et al.* [32]. ©AAS. Reproduced with permission.

[36] suggest that the bump draws its energy from the Ly α radiation field. Specifically, these authors suggest that the Ly α -driven dissociation of water in the inner disk generates a population of highly non-thermal H₂ and emission from this population then produces the 1600 Å-Bump, i.e., efficient water dissociation by Ly α photons during the later stages of disk dispersal [36]. This scenario is supported by the lack of a correlation between 1600 Å-Bump and stellar X-ray luminosity [96]. Another cause for large 1600 Å-Bump luminosities may be high photo-electron densities (presumably driven by stellar X-rays; [94,95]).

4.3. Disk Absorption

For moderately inclined disks ($i \gtrsim 70^\circ$), the line of sight towards the central star passes through the upper disk regions. The observed spectrum then contains absorption features from the disk. In the FUV, the two most abundant species in protoplanetary disks, H₂ and CO, have strong absorption bands, which allow the measurements of column densities and rovibrational temperatures. The absorption profile depends on (1) an (assumed) turbulent velocity (typically small, $\sim 0.1 \text{ km}^{-1}$), (2) a column density, and (3) a rotational temperature.

While FUV-CO absorption is an established technique in many fields of astronomy, e.g., for the study of the interstellar medium (ISM, see [97] and references therein) or planets [98], its use for protoplanetary disks was first proven in 2011 by France *et al.* [32], who measure absorption by the ground vibrational state ($v=0$) of CO against the backlight of the FUV accretion continuum of the central star. In their analysis of 34 T Tauri stars, McJunkin *et al.* [99] find CO absorption in about one quarter of the sources. For these sources, the FUV-CO absorption velocities are compatible with the radial velocity of the target star within the instrumental velocity calibration uncertainty of about 15–20 km s^{-1} . The data imply rotational temperatures around 500 K, which may be reached out to radii of 0.2–2 au assuming thermal equilibrium with the stellar radiation field. Compared to the IR-CO emission, the temperatures of the UV-CO absorption are lower, perhaps because FUV-CO absorption traces a gas population at larger disk radii than the IR data. When combined with estimates for the conditions required for a thermal equilibrium between the rotational states and the radiation field from disk models [100], McJunkin *et al.* [99] suggest that the CO absorbing gas resides in disk layer at a height of $z/r \sim 0.6$ and 0.7, i.e., the flared upper disk atmosphere.

In the FUV spectra of CTTSs, H₂ absorption is seen both, against the continuum and against the Ly α line. For estimating an CO/H₂-ratio, however, one should compare the respective absorption features seen against the continuum [see discussion in 101]. In the best characterized CO and H₂ absorption system, RW Aur, the CO/H₂ ratio is found to be $\approx 10^{-4}$, which is compatible with the value for the ISM. Since the

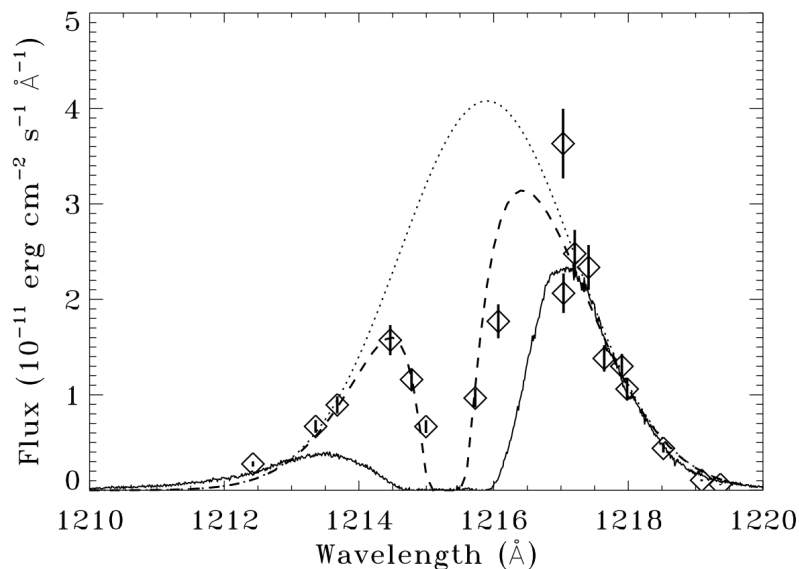


Figure 9. Example of a Ly α reconstruction based on H₂ fluxes. Diamonds indicate the wavelengths at which measured H₂ progressions are pumped, the dashed line indicates an H₂ model for T=2500 K and $\log N(\text{H}_2) = 18.5$ and a surface filling factor for the H₂ material as seen by the Ly α emitting region. In this model, the intrinsic Ly α line is Gaussian-shaped (dotted), the H₂ gas sees the dashed profile, and the Ly α profile observed by HST is subject to additional interstellar absorption (solid line). From Herczeg *et al.* [82]. ©AAS. Reproduced with permission.

CO/H₂ is of fundamental importance for disk chemistry and disk mass estimates, future studies using FUV absorption will provide unique information not attainable with, e.g., ALMA observations and disk modeling. Therefore, future mission concepts like NASA's LUVOIR specifically aim at high-sensitivity, high-resolution absorption line spectroscopy through moderately inclined disks [102].

4.4. Disk Chemistry and the UV SED

The strength and shape of the FUV radiation field has a strong influence on the chemical abundances of the disk, both at planet-forming radii [$r < 10$ au; 94,103] and at larger radii ($r > 50$ au) where the majority of the disk mass resides [104]. The stellar FUV continuum controls the dissociation of the most abundant disk molecules (H₂ and CO; [105,106]). The propagation of the FUV continuum is mainly regulated by dust grains [107]; the processes of grain-growth and settling likely allow these photons to penetrate deeper into the disk as the protoplanetary environment evolves [108].

Bergin *et al.* [94] first emphasized the importance of accretion-generated H I Ly α to the disk chemistry, and more recently it has been shown that the FUV spectral energy distribution of all CTTSs is overwhelmingly dominated ($\gtrsim 80\%$) by Ly α emission [31,101]. Unlike the FUV continuum emission, the radiative transfer of Ly α photons is controlled mainly by resonant scattering in the upper, atomic disk atmosphere [109]. Subsequent detailed disk modeling has demonstrated the importance of properly accounting for Ly α radiation from the central star, finding significant ($\gtrsim 1$ order of magnitude) depletions in the abundances of C₂H₄, CH₄, HCN, NH₃, and SO₂ when Ly α is included [110]. Interestingly, some species with large photo-absorption cross-sections in the region around Ly α , such as H₂O, do not show significant depletion, because the enhanced dissociation rate is balanced by Ly α -driven photodesorption of water molecules from dust grains. It is clear now that Ly α is a mandatory component of FUV radiation

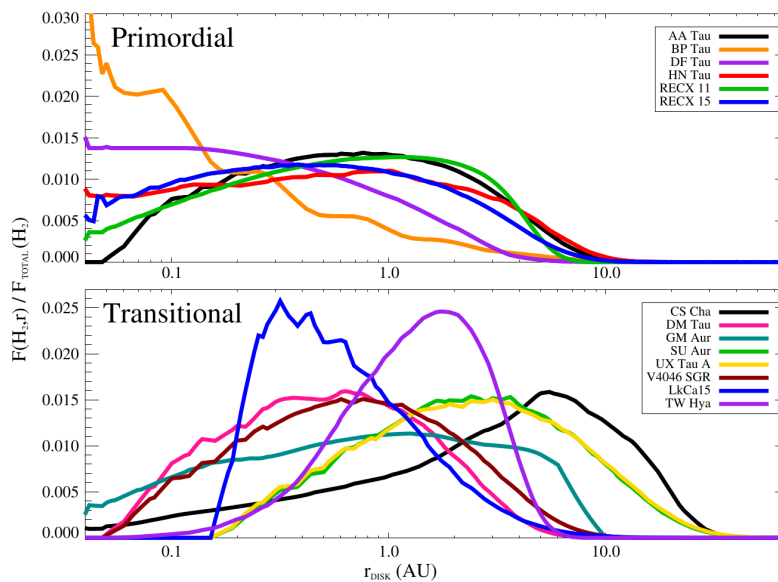


Figure 10. Comparison of full and transitional disks in their reconstructed radial distributions of the observed H_2 emission. From Hoadley *et al.* [84]. ©AAS. Reproduced with permission.

fields used for chemical modeling. Historically, the large CTTS spectral atlases do not cover $Ly\alpha$ [61], or are dominated by geocoronal emission, such as archival IUE data. Reconstructing the $Ly\alpha$ radiation field impinging the inner disk region requires measurements of a large number of UV- H_2 lines (see Fig. 9); the largest such atlas of high-resolution FUV spectra of CTTSs is provided by France *et al.* [101] with high-level data available for download.

Deriving accurate FUV fluxes is challenging, because extinction estimates are typically based on the comparison between a stellar template (augmented by a suitable accretion spectrum for CTTSs) and observed colors or flux-calibrated spectra plus an assumed shape of the extinction curve. It is known that the extinction values derived from optical and NIR data can differ, but this effect is mild compared to the extrapolation into the FUV where the correction factors are large. Specifically, it was found that the intrinsic, de-reddened UV- H_2 luminosity is correlated with the assumed extinction values, which is not physically expected and suggests that the large extinction corrections, or rather errors in them, dominate over the intrinsic variations between the systems [36]. In an attempt to remedy this situation, McJunkin *et al.* [111] performed detailed modelling of the UV- H_2 lines including self-absorption and use the known branching ratios to recover the shape of the FUV extinction curve. Although the line of sight towards the UV- H_2 emitting region in the inner disk may be subject to a different extinction than the central star, McJunkin *et al.* [111] find a number of sources for which this and more traditional methods agree, but they also find systems for which both methods strongly disagree and more investigation on the subject of FUV extinction curves relevant for CTTSs is needed.

4.5. Disk dispersal

Primordial gas disks are known to dissipate on timescales of $\lesssim 10$ Myr, at which point mass accretion onto the central star halts [112]. At some time in the evolution of protoplanetary disks thermal winds carry away more mass than is transported inwards, which leads to the dispersal of the disk from the inside-out [113]. Inner gas disks may survive longer than the typical ~ 3 Myr lifetime of inner dust disks (e.g., [86,91]). The detailed physical process that clears the inner disk are not yet established. Among the

proposed mechanisms are photoevaporation [113,114] and dynamical clearing by exoplanetary systems [115], possibly aided by the magnetorotational instability [116].

Models that simultaneously treat FUV, EUV, and X-ray irradiation from the central star have shown that the FUV illumination can control the total evaporation rate (and hence the disk lifetime) by driving the heating at intermediate ($r \sim 3 - 30$ au) and large radii ($r \geq 100$ au, [114]). FUV radiation also controls the gas temperature at the base of the evaporative flows through the generation of photoelectrons released by FUV-illuminated dust grains. Grain-growth and dust settling during the first stages of the planet formation process enable deeper penetration of the FUV radiation.

UV photons not only regulate disk dispersal, but are also powerful diagnostics thereof. For example, UV- H_2 emission is sensitive to gas surface densities lower than $10^{-6} \text{ g cm}^{-2}$ [83], making them an extremely useful probe of remnant gas during the late stages of disk dispersal. Hoadley *et al.* [84] study the radial distribution of the UV- H_2 using kinematic modelling of the H_2 profiles. In particular, these authors compare the radial distributions of full and transitional disks (Fig. 10) finding that the distribution in transitional disks is shifted towards larger radii. The H_2 and CO gas populations decline with dust disk dissipation [88,117], but the H_2 depletion lags behind the CO for disks with large inner dust cavities [118].

5. Jets and outflows

CTTSs, and their younger siblings, the class 0 and I sources, drive outflows and jets (collimated outflows, see Frank *et al.* [119] for a recent review). The origin of the various outflow components is not clear and different parts of the young stellar system may contribute with varying fractions depending on the actual tracer (Fig. 2). Specifically, the star itself may drive a stellar wind [120], the region (magnetically) connecting the star and the disk may eject a so-called X-wind [121], and the disk itself may launch a disk wind [122].

Outflows and jets are traditionally studied in forbidden emission lines tracing thin ($\log n \sim 2 \dots 4$ in units of cm^{-3}) plasma with temperatures around 10^4 K and spectacular jet images exist, which show beautiful phenomena such as bow shocks, wiggling, and precession (e.g., [123]). The jet emission is usually concentrated in so-called knots where the jet material has been shock heated and is now seen in emission lines. These knots move along the jet axis away from the driving source. Cooler jet components are seen as molecular emission lines, which can be studied at radio-frequencies even for highly embedded sources [124,125]. In recent years, the observing window for jet studies opened significantly and now spans from the highest photon energies in the X-ray regime [126–128] down to m-wavelength radiation [129].

Despite this large arsenal of observing opportunities, FUV observations of jets are highly powerful, because they allow us to measure (a) the molecular content through H_2 emission lines ($T \sim 10^3$ K) and (b) kinematically resolve the hot jet in high excitation lines like C IV ($T \sim 10^5$ K) with very high angular resolution below 0.1 arcsec [33]. Often, there is indirect evidence for an outflow component in, e.g., C IV. Dupree *et al.* [130] suggest that a hot ($\sim 10^5$ K) wind exists in TW Hya based on a roughly P Cygni-like asymmetry observed in hot lines like C III, C IV, and O VI. The absorption extends out to blue-shifted velocities of up to 400 km s^{-1} and Dupree *et al.* [130] estimate that a mass-loss rate of roughly 10% of the accretion rate may be sufficient to cause the observed absorption signals. This interpretation, however, heavily relies on the assumption that the intrinsic line profiles are symmetric and that the asymmetry is indeed caused by absorption. Johns-Krull [50] dispute this assumption and show that other features in the line profiles that would be expected in a hot wind scenario are not present. They suggest that there is no indication for absorption by a hot wind in TW Hya, only for absorption in low ionization lines by a comparably cold wind is seen.

While these arguments address a hot stellar wind, jet emission in C IV is directly observed and there is often also indirect evidence for such a hot jet, e.g., strong emission seen in IUE data but not in smaller

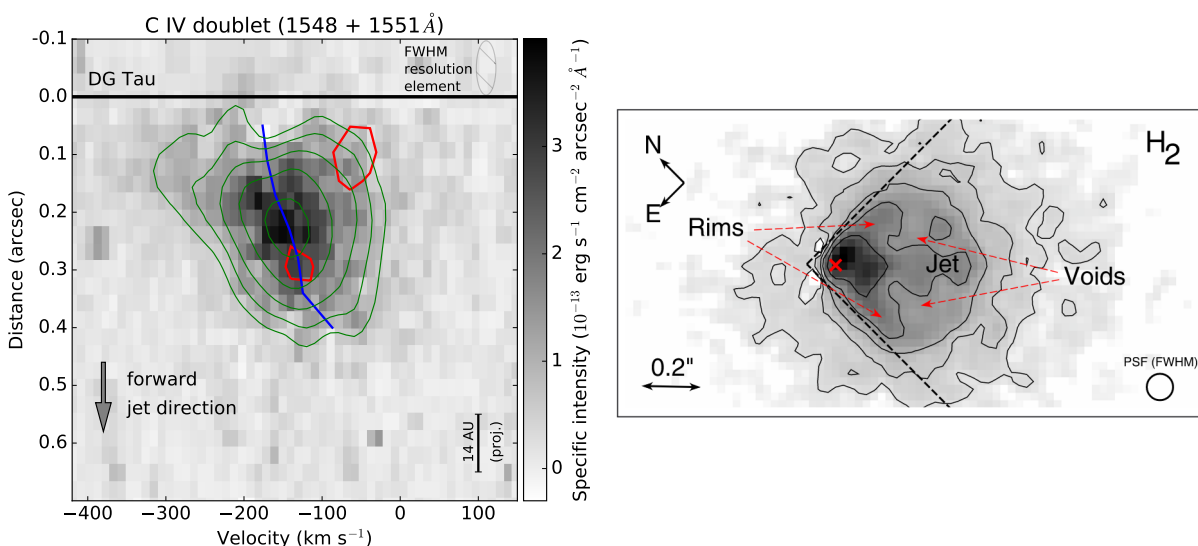


Figure 11. **Left:** Position-Velocity diagram for the C IV emission of the DG Tau jet. The red contours indicate emission components seen in traditional tracers like [O I]. Note that there is no emission at the stellar position and all C IV emission originates within the jet. From Schneider *et al.* [33]. **Right:** Image of UV- H_2 of DG Tau. Reproduced with permission © ESO.

aperture HST data or the hot lines exhibit a similar kinematic morphology as forbidden lines that trace the jet rather than accretion. Studies using long-slit data were initiated based on these indirect indications.

It was found that the jet's C IV emission is typically observed to be offset from the star along the forward facing (approaching) jet by tens of au (see Fig. 11). Since C IV and X-ray emission spatially overlap, it is natural to assume that they probe the same jet component [33]. The mass-loss associated with the C IV emission is somewhere between total mass-loss and the mass-loss related to the X-ray emission [131].

Both, the X-ray and the C IV were not predicted by models and there is no consensus on their origin. There are, however, a number of observational constraints that set these jet features apart from the well known optical jet. First, the C IV and X-ray emission are stationary so that heating by the same shocks that cause the optical knots is unlikely [132]. Second, adiabatic cooling would have lowered the temperature of outflowing material with any reasonable initial temperature ($T < 10^7$ K) below C IV emitting temperatures so that local heating is required to power the C IV and X-ray emission at the measured distance of tens of au. Third, the velocity of the C IV emission is comparable to that of the bulk of the optical jet but spatially offset indicating a different heating mechanism than shocks. Schneider *et al.* [33] speculate that magnetic heating similar to processes in the stellar coronae may be responsible for the C IV and X-ray emission. In addition, a velocity just slightly higher than the optical jet suggests that this outflow originates in the inner disk region, i.e., extends the jet's onion-like velocity structure to the innermost regions very close to the star where stellar and disk magnetic fields interact. C IV from protostellar jets may therefore be a powerful probe of the magnetic field in an accretion funnel region.

In addition to the very hot jet, FUV observations also trace the jet's molecular hydrogen emission [133,134]. This UV- H_2 emission is caused by the very same processes that cause UV- H_2 disk emission (cf. sect. 4.1), i.e., fluorescent emission pumped by Ly α photons. The wide-angle structure seen in UV- H_2 (Fig. 11 right) appears stationary and agrees very well with the spatial morphology of the H_2 emission seen in the NIR with AO-equipped IFUs [135]. The molecular outflow appears stationary in time contrasting the moving knots seen in optical data of protostellar jets. Thus, the UV- H_2 likely arises in a wind region

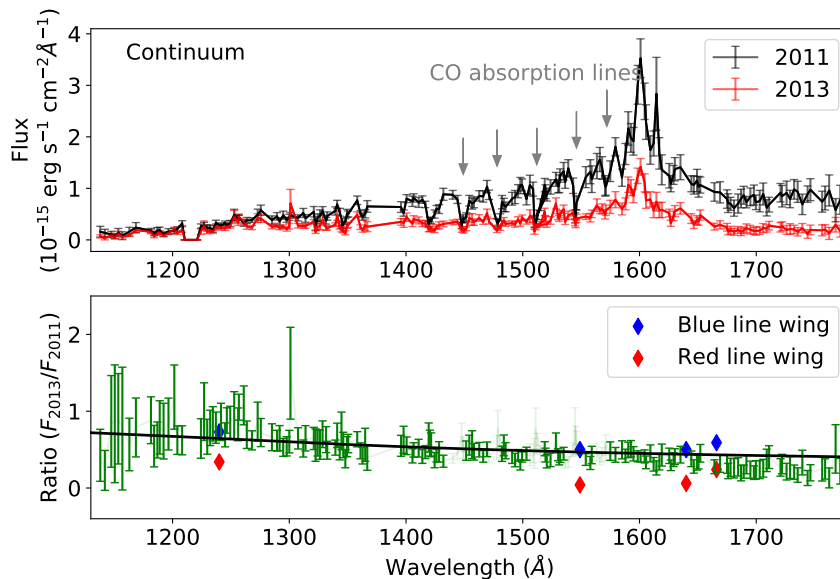


Figure 12. Top: FUV continuum spectra of AA Tau during bright and dim states. **Bottom:** Ratio between bright and dim states with the evolution of emission lines shown in blue/red diamonds for the blue and red line wing, respectively. Notable is the bluer appearance of the continuum during the dim state, which is incompatible with just extra absorption and more compatible with scattering. From Schneider *et al.* [89]. Reproduced with permission © ESO.

heated by ambipolar diffusion with subsequent pumping by stellar Ly α photons and likely traces probably the outermost regions of the MHD wind [134].

6. Variability

In the previous sections, we described how FUV emission can originate from chromospheric activity, from accretion, and from outflows or jets. All of these sources are variable, just on different time scales. Given the general sparsity of FUV observations (since space-based instrumentation is required) and the fact that, compared with other wavebands, relatively low column densities of intervening material absorb nearly all intrinsic signal, variability in the FUV band is not well-studied.

One characteristic time scale in stars is the rotation period. Active regions or accretion spots rotate in and out of view. This accounts partially for observed changes in the accretion rate with time [136]. Early IUE monitoring of DI Cep and BP Tau shows that this holds true in the UV. FUV line fluxes in DI Cep associated with the accretion hot spot change over the course of a rotational cycle and additionally line and continuum fluxes change as the accretion rate changes when comparing spectra taken more than a decade apart. These changes are correlated with the *V* band magnitude [137]. Similarly, in BP Tau emission lines that are formed through recombination, i.e. in the accretion shock, such as O I and He II vary with stellar phase, while lines that can be formed both in the accretion shock and in the transition region, such as the C IV doublet at 1548 and 1550 Å, show less pronounced phase variation [138,139]. In a more recent observation of GM Aur model fits allow to disentangle accretion rate and spot area, indicating that, at least on this star, it is in fact the density of the accretion stream, that changes, not the size of the shock [140].

It is worth noting that the shock is also invoked as the source of soft X-ray emission [141–143], yet X-ray and FUV flux appear uncorrelated [96]. This might be related to another key finding, namely that

accretion rates derived from X-rays fall short of those derived from UV/optical tracers by an order of magnitude [144]. Conceptually, the FUV and the soft X-rays should be the best tracers for the accretion rate, because both the FUV and the X-ray emission is produced very close to the accretion shock where the energy budget is dominated by the kinetic energy of the infalling mass. The X-ray emission is formed right after the material passes through the shock front. Models successfully reproduce line ratios in the spectrum [141,145], although they do not describe the full temperature range of the shock accurately [143]. The FUV emission is formed at the bottom of the accretion column and in the gas around it [52,71] and yet, X-ray and FUV variability seem uncorrelated or even anti-correlated [75]. This finding clearly points to a fundamental problem in our current understanding of the accretion shock.

What is the impact of this variability on the FUV emission from the disk? Section 4.2 discusses the 1600 Å bump, which is most likely due to emission from excited H₂, i.e. it originates in the disk. In a sample of five CTTSs observed five times each with HST/STIS, the flux of this feature correlates with the accretion luminosity determined from the UV continuum [96], but not with the X-ray flux. This is consistent with the idea that the H₂ is excited by the stellar Ly α emission.

Another disk related feature that has a great impact on the FUV appearance of CTTSs are long-lasting dimming events such as the one observed for AA Tau [146]. During such dimming events, the optical brightness of the system decreases by a few magnitudes for months to years, i.e., they are significantly dimmer for a longer time-period than typically observed. While the precise cause for the dimming is not clear, it is likely caused by changes in the inner disk structure, precisely the disk region traced by UV-H₂ emission (see sect. 4.1). Therefore, comparison of the UV-H₂ emission before and during a dimming event provides key information on the disk regions that take part in the dimming event. Schneider *et al.* [89] find that the observed UV-H₂ line profiles lack emission from regions within 2 au from the star while emission originating at larger radii is unaffected [also 84]. Furthermore, Schneider *et al.* [89] find that the flux ratio between the dim and bright state cannot be explained by simply adding extra absorption for both, the continuum and the red line wings of hot ion lines (see Fig. 12). These authors suggest that scattering is the most plausible explanation, because other scenarios require uncomfortable fine-tuning, e.g., anomalous dust requires not only a very peculiar dust size distribution, but also an exchange of a precise fraction of dust obscuring the system during the bright state with a special dust column. Lastly, the blue line wings of hot ion lines are only weakly affected by the dimming suggesting that they have strong outflow/jet contributions already in the bright state. Such dimming events therefore provide unique information as the central star is hidden behind a natural coronagraph. Unfortunately, these dimming events are rare and unpredictable so that following each new discovery would be highly valuable.

Young stars also exhibit much longer lasting and more consequential outbursts, where the disk structure changes dramatically and the accretion rate increases by several orders of magnitude. The longest and brightest of these outbursts are called “FU Ori outbursts”, and it can take decades or centuries until the accretion rate settles back to the previous, stable state (see review in [147]). In FU Ori outbursts, the system is totally dominated by the accretion luminosity. The UV spectrum looks very different from a CTTS: It appears to be a superposition of a hot (9000 K), geometrically thick inner disk and a cooler outer component (5000 K), dominated by a dense forest of absorption lines from disk outflows [148,149].

In outflows and jets, we see temporal variability in the mass launching. In the jets, distinct emission regions, called “knots”, can be seen, which are either blobs of mass launched from the star over periods of years or shock fronts traveling along the slower moving material of the jet. One of the best examples of this in the FUV is the jet of HD 163296, a Herbig Ae star. This star shares many characteristics with CTTSs, but because it is more massive, and thus brighter, the accretion and jet features can be observed with comparably higher signal-to-noise ratios. Repeated observations of Ly α emission in the jets shows that knots observed at one period faint away and new knots emerge from the source of the jet [150,151]. Similar observations have been made for CTTSs in other bands (e.g. in DG Tau four knots have been tracked for

two decades in the optical, X-ray and radio [152]), so it is likely that a time-series of Ly α images would show the flow of the knots along the jets in CTTs, too, if they were observed with a sufficiently sensitive instrument.

7. Conclusions and Outlook

Young stars are strong UV emitters compared to their older siblings. This emission is mostly due to processes that are intrinsic to star formation, namely, protostellar mass accretion, enhanced stellar activity, and emission from surrounding disks and outflows. In addition, the UV radiation field controls the conditions in the planet forming region of protoplanetary disks and is thought to drive or contribute to the eventual dispersal of the disks. Therefore, UV observations are critical to painting the complete picture of star- and planet-formation.

In this review, we have discussed, first, that the chromospheric and transition region emission is particularly strong in CTTs due to enhanced magnetic activity as young stars are generally fast rotators. Second, we showed that the accretion processes releases most of the energy in the UV range as continuum and Ly α emission. Accretion also causes strong emission lines from hot ions (e.g. C IV), which provide detailed accretion kinematics not available in other wavelength ranges. Their study suggests that accretion funnels are not homogeneous structures but rather stratified in density so that optical depth effects are important and probably only a fraction of the accretion funnel is seen depending on inclination angle. Third, UV observations provide important, complementary diagnostics for the structure and evolution of protoplanetary disks and, fourth, jets and outflows are also seen in the UV regime where new observations revealed jet components not seen in traditional jet tracers, namely a hot, stationary jet component close to the central star. Fifth, young stars are highly variable and monitoring campaigns combining X-ray, UV, and optical data are beginning to disentangle how the individual features are causally related. Despite all this success, there is no theory that can self-consistently explain all features. The coming years will see increasingly sophisticated models, incorporating, e.g., a more detailed treatment of the radiative effects of the accretion funnel including the reprocessing of the primary X-ray photons.

While most of the contributions to the system's FUV emission have now been identified, there are still potentially large uncertainties that need to be addressed by future observations. First, scattering may be important in more obscured sources or sources seen under high inclination angles [89]; it is currently unknown how much scattering contributes to the observed UV spectrum of a CTT. This is important, because the de-reddening corrections that apply to the central star may not apply to other FUV emission components. High sensitivity two-dimensional imaging spectroscopy (e.g., an IFU or MSA-enabled instrument) would allow us to simultaneously measure the inner disk region as a function of wavelength, spatial location, and velocity; allowing us to quantify the relative importance of scattering and the temporal variability of different disk components individually. Second, jets can contribute to the FUV emission and, because their emission is located close to the star, their emission can be mistaken as stellar; note that there are not necessarily kinematic signatures like highly blue-shifted emission as the blue- and red-shifted jet lobe may both emit resulting in a net velocity shift close to zero. Future high resolution imaging spectroscopy observations are needed to constrain the importance of scattering and jet emission in "typical" samples of CTTs.

The next major step for understanding the UV emission of CTTs will be the Hubble Space Telescope's ULLYSES program. The ULLYSES program will dedicate ~ 500 orbits to the study of low-mass star formation in the UV. ULLYSES will include a spectral atlas of ~ 60 new sources and a dedicated, multi-wavelength monitoring program for high-priority targets. On intermediate time scales, however, neither ESA nor NASA are committed to build a space mission with dedicated UV instrumentation within the next decade. The Russian Spektr-UV mission may be the next dedicated UV mission and is

currently scheduled to launch in the mid-2020s. With a 1.7 m mirror, it will be somewhat comparable to HST; also in its spectroscopic and imaging capabilities (low- and high-resolution UV spectroscopy). The next opportunity to launch a large space mission with sensitive UV spectroscopic capabilities may be the LUVOIR mission concept [153,154], to be launched in the late 2030s. In fact, LUVOIR's science goals specifically include the questions of low-mass star formation that we discussed in the review.

Author Contributions: writing–review and editing, P.C.S., H.M.G, K.F.; visualization, P.C.S.

Funding: This research was funded by DLR grant number 50 OR 1907. K.F. acknowledges support for this work from HST GO programs 14604, 14703, and 15070. The authors also express their gratitude to N. Arulanantham for providing information on the H₂ emission properties of CTTs.

Conflicts of Interest: The authors declare no conflict of interest.

References

1. Imhoff, C.L. An historical perspective. In search of the T tauri stars. *Astronomy Quarterly* **1977**, *1*, 213–238. doi:10.1016/S0364-9229(77)80009-2.
2. Joy, A.H. T Tauri Variable Stars. *ApJ* **1945**, *102*, 168. doi:10.1086/144749.
3. Greenstein, J.L. A Possible Energy Source for T Tauri Stars. *PASP* **1950**, *62*, 156. doi:10.1086/126264.
4. Henyey, L.G.; Lelevier, R.; Levée, R.D. The Early Phases of Stellar Evolution. *PASP* **1955**, *67*, 154. doi:10.1086/126791.
5. Ambartsumian, V.A. On the Origin of Stars. Liege International Astrophysical Colloquia, 1954, Vol. 5, p. 293.
6. Walker, M.F. Studies of extremely young clusters. I. NGC 2264. *ApJ* **1956**, *124*, 668–668.
7. Magazzu, A.; Rebolo, R.; Pavlenko, I.V. Lithium Abundances in Classical and Weak T Tauri Stars. *ApJ* **1992**, *392*, 159. doi:10.1086/171414.
8. Pinsonneault, M. Mixing in Stars. *ARA&A* **1997**, *35*, 557–605. doi:10.1146/annurev.astro.35.1.557.
9. Kuhi, L.V. Spectral energy distributions of T Tauri stars. *A&As* **1974**, *15*, 47–89.
10. Strom, S.E.; Strom, K.M.; Grasdalen, G.L. Young stellar objects and dark interstellar clouds. *ARA&A* **1975**, *13*, 187–216. doi:10.1146/annurev.aa.13.090175.001155.
11. Kuhi, L.V. Ultraviolet Continuous Emission in T Tauri Stars. *PASP* **1966**, *78*, 430. doi:10.1086/128380.
12. Kuhi, L.V. Optical Observations of Very Young Stars. *Interstellar Ionized hydrogen Proceedings of the Symposium on HII*; Terzian, Y., Ed., 1968, p. 13.
13. Cram, L.E. Atmospheres of T Tau stars : the photosphere and low chromosphere. *ApJ* **1979**, *234*, 949–957. doi:10.1086/157578.
14. Dumont, S.; Heidmann, N.; Kuhi, L.V.; Thomas, R.N. Chromospheres of T Tauri-type stars. *A&A* **1973**, *29*, 199.
15. Brown, A.; de M. Ferraz, M.C.; Jordan, C. The chromosphere and corona of T Tauri. *MNRAS* **1984**, *207*, 831–859. doi:10.1093/mnras/207.4.831.
16. Calvet, N.; Basri, G.; Kuhi, L.V. The chromospheric hypothesis for the T Tauri phenomenon. *ApJ* **1984**, *277*, 725–737. doi:10.1086/161744.
17. Walker, M.F. A Possible Interpretation of the Ultraviolet Excess Stars. *AJ* **1963**, *68*, 298. doi:10.1086/109056.
18. Kuhi, L.V. Mass Loss from T Tauri Stars. *ApJ* **1964**, *140*, 1409. doi:10.1086/148047.
19. Larson, R.B. Processes in Collapsing Interstellar Clouds. *ARA&A* **1973**, *11*, 219. doi:10.1146/annurev.aa.11.090173.001251.
20. Walker, M.F. Studies of Extremely Young Clusters.VI. Spectroscopic Observations of the Ultraviolet-Excess Stars in the Orion Nebula Cluster and NGC 2264. *ApJ* **1972**, *175*, 89. doi:10.1086/151540.
21. Cohen, M.; Kuhi, L.V. Observational studies of pre-main-sequence evolution. *ApJs* **1979**, *41*, 743–843. doi:10.1086/190641.
22. Dullemond, C.P.; Monnier, J.D. The Inner Regions of Protoplanetary Disks. *ARA&A* **2010**, *48*, 205–239, [arXiv:astro-ph.SR/1006.3485]. doi:10.1146/annurev-astro-081309-130932.

23. Williams, J.P.; Cieza, L.A. Protoplanetary Disks and Their Evolution. *ARA&A* **2011**, *49*, 67–117, [[arXiv:astro-ph.GA/1103.0556](#)]. doi:10.1146/annurev-astro-081710-102548.
24. Lynden-Bell, D.; Pringle, J.E. The evolution of viscous discs and the origin of the nebular variables. *MNRAS* **1974**, *168*, 603–637. doi:10.1093/mnras/168.3.603.
25. Shakura, N.I.; Sunyaev, R.A. Reprint of 1973A&A...24..337S. Black holes in binary systems. Observational appearance. *A&A* **1973**, *500*, 33–51.
26. Ulrich, R.K. An infall model for the T Tauri phenomenon. *ApJ* **1976**, *210*, 377–391. doi:10.1086/154840.
27. Bertout, C. The accretion disk paradigm for young stars. *Star-Disk Interaction in Young Stars*; Bouvier, J.; Appenzeller, I., Eds., 2007, Vol. 243, *IAU Symposium*, pp. 1–12. doi:10.1017/S1743921307009362.
28. Imhoff, C.L.; Giampapa, M.S. The ultraviolet spectrum of the T Tau star RW Aur. *ApJl* **1980**, *239*, L115–L119. doi:10.1086/183305.
29. Appenzeller, I.; Wolf, B. The satellite-UV spectrum of S CrA. *A&A* **1979**, *75*, 164–169.
30. Herczeg, G.J.; Linsky, J.L.; Valenti, J.A.; Johns-Krull, C.M.; Wood, B.E. The Far-Ultraviolet Spectrum of TW Hydrae. I. Observations of H₂ Fluorescence. *ApJ* **2002**, *572*, 310–325, [[arXiv:astro-ph/0201319](#)]. doi:10.1086/339731.
31. Schindhelm, E.; France, K.; Herczeg, G.J.; Bergin, E.; Yang, H.; Brown, A.; Brown, J.M.; Linsky, J.L.; Valenti, J. Ly α Dominance of the Classical T Tauri Far-ultraviolet Radiation Field. *ApJl* **2012**, *756*, L23, [[arXiv:astro-ph.SR/1208.2271](#)]. doi:10.1088/2041-8205/756/1/L23.
32. France, K.; Schindhelm, E.; Burgh, E.B.; Herczeg, G.J.; Harper, G.M.; Brown, A.; Green, J.C.; Linsky, J.L.; Yang, H.; Abgrall, H.; Ardila, D.R.; Bergin, E.; Bethell, T.; Brown, J.M.; Calvet, N.; Espaillat, C.; Gregory, S.G.; Hillenbrand, L.A.; Hussain, G.; Ingleby, L.; Johns-Krull, C.M.; Roueff, E.; Valenti, J.A.; Walter, F.M. The Far-ultraviolet “Continuum” in Protoplanetary Disk Systems. II. Carbon Monoxide Fourth Positive Emission and Absorption. *ApJ* **2011**, *734*, 31, [[arXiv:astro-ph.EP/1104.0670](#)]. doi:10.1088/0004-637X/734/1/31.
33. Schneider, P.C.; Eisloffel, J.; Güdel, M.; Günther, H.M.; Herczeg, G.; Robrade, J.; Schmitt, J.H.M.M. HST FUV C iv observations of the hot DG Tauri jet. *A&A* **2013**, *550*, L1, [[arXiv:astro-ph.SR/1212.6363](#)]. doi:10.1051/0004-6361/201118592.
34. van Duinen, R.J.; Aalders, J.W.G.; Wesseliuss, P.R.; Wildeman, K.J.; Wu, C.C.; Luinge, W.; Snel, D. The ultraviolet experiment onboard the Astronomical Netherlands Satellite - ANS. *A&A* **1975**, *39*, 159–163.
35. de Boer, K.S. Far-UV observations of T Tau-like stars. *A&A* **1977**, *61*, 605–608.
36. France, K.; Roueff, E.; Abgrall, H. The 1600 Å Emission Bump in Protoplanetary Disks: A Spectral Signature of H₂O Dissociation. *ApJ* **2017**, *844*, 169, [[arXiv:astro-ph.SR/1706.09940](#)]. doi:10.3847/1538-4357/aa7cee.
37. Boggess, A.; Carr, F.A.; Evans, D.C.; Fischel, D.; Freeman, H.R.; Fuechsel, C.F.; Klinglesmith, D.A.; Krueger, V.L.; Longanecker, G.W.; Moore, J.V. The IUE spacecraft and instrumentation. *Nature* **1978**, *275*, 372–377. doi:10.1038/275372a0.
38. Gahm, G.F.; Fredga, K.; Liseau, R.; Dravins, D. The far-UV spectrum of the T Tauri star RU Lupi. *A&A* **1979**, *73*, L4–L6.
39. Bouvier, J.; Bertout, C.; Benz, W.; Mayor, M. Rotation in T Tauri stars. I. Observations and immediate analysis. *A&A* **1986**, *165*, 110–119.
40. Bouvier, J.; Cabrit, S.; Fernandez, M.; Martin, E.L.; Matthews, J.M. COYOTES I : the photometric variability and rotational evolution of T Tauri stars. *A&A* **1993**, *272*, 176–206.
41. Herbst, W.; Eisloffel, J.; Mundt, R.; Scholz, A. The Rotation of Young Low-Mass Stars and Brown Dwarfs. *Protostars and Planets V*; Reipurth, B.; Jewitt, D.; Keil, K., Eds., 2007, p. 297, [[arXiv:astro-ph/0603673](#)].
42. Bouvier, J.; Matt, S.P.; Mohanty, S.; Scholz, A.; Stassun, K.G.; Zanni, C. Angular Momentum Evolution of Young Low-Mass Stars and Brown Dwarfs: Observations and Theory. *Protostars and Planets VI*; Beuther, H.; Klessen, R.S.; Dullemond, C.P.; Henning, T., Eds., 2014, p. 433, [[arXiv:astro-ph.SR/1309.7851](#)]. doi:10.2458/azu_uapress_9780816531240-ch019.
43. Gregory, S.G.; Jardine, M.; Gray, C.G.; Donati, J.F. The magnetic fields of forming solar-like stars. *Reports on Progress in Physics* **2010**, *73*, 126901, [[arXiv:astro-ph.SR/1008.1883](#)]. doi:10.1088/0034-4885/73/12/126901.

44. Houdebine, E.R.; Mathioudakis, M.; Doyle, J.G.; Foing, B.H. Observation and modelling of main sequence star chromospheres. V. Ultraviolet excess emission in active M dwarfs. *A&A* **1996**, *305*, 209.
45. Feigelson, E.D.; Montmerle, T. High-Energy Processes in Young Stellar Objects. *ARA&A* **1999**, *37*, 363–408. doi:10.1146/annurev.astro.37.1.363.
46. Walter, F.M. The naked T Tauri stars : the low-mass pre-main sequence unveiled. *PASP* **1987**, *99*, 31–37. doi:10.1086/131952.
47. Ingleby, L.; Calvet, N.; Bergin, E.; Herczeg, G.; Brown, A.; Alexander, R.; Edwards, S.; Espaillat, C.; France, K.; Gregory, S.G.; Hillenbrand, L.; Roueff, E.; Valenti, J.; Walter, F.; Johns-Krull, C.; Brown, J.; Linsky, J.; McClure, M.; Ardila, D.; Abgrall, H.; Bethell, T.; Hussain, G.; Yang, H. Near-ultraviolet Excess in Slowly Accreting T Tauri Stars: Limits Imposed by Chromospheric Emission. *ApJ* **2011**, *743*, 105, [arXiv:astro-ph.SR/1110.6312]. doi:10.1088/0004-637X/743/2/105.
48. Costa, V.M.; Lago, M.T.V.T.; Norci, L.; Meurs, E.J.A. T Tauri stars: The UV/X-ray connection. *A&A* **2000**, *354*, 621–635.
49. Findeisen, K.; Hillenbrand, L.; Soderblom, D. Stellar Activity in the Broadband Ultraviolet. *AJ* **2011**, *142*, 23, [arXiv:astro-ph.SR/1105.1377]. doi:10.1088/0004-6256/142/1/23.
50. Johns-Krull, C.M. The Magnetic Fields of Classical T Tauri Stars. *ApJ* **2007**, *664*, 975–985, [arXiv:astro-ph/0704.2923]. doi:10.1086/519017.
51. Koenigl, A. Disk Accretion onto Magnetic T Tauri Stars. *ApJl* **1991**, *370*, L39. doi:10.1086/185972.
52. Calvet, N.; Gullbring, E. The Structure and Emission of the Accretion Shock in T Tauri Stars. *ApJ* **1998**, *509*, 802–818. doi:10.1086/306527.
53. Schneider, P.C.; Günther, H.M.; Robrade, J. Stellar X-ray accretion signatures. *Astronomische Nachrichten* **2017**, *338*, 201–206. doi:10.1002/asna.201713331.
54. Hartmann, L.; Herczeg, G.; Calvet, N. Accretion onto Pre-Main-Sequence Stars. *ARA&A* **2016**, *54*, 135–180. doi:10.1146/annurev-astro-081915-023347.
55. Simon, T.; Vrba, F.J.; Herbst, W. The Ultraviolet and Visible Light Variability of BP Tauri: Possible Clues for the Origin of T Tauri Star Activity. *AJ* **1990**, *100*, 1957. doi:10.1086/115651.
56. Gómez de Castro, A.I.; Fernández, M. Ultraviolet spectroscopy of the hotspot in the classical T Tauri star DI Cep: observational indications of magnetically channelled accretion. *MNRAS* **1996**, *283*, 55–65. doi:10.1093/mnras/283.1.55.
57. Gómez de Castro, A.I.; Franqueira, M. Accretion and UV Variability in BP Tauri. *ApJ* **1997**, *482*, 465–469. doi:10.1086/304149.
58. Johns-Krull, C.M.; Valenti, J.A.; Linsky, J.L. An IUE Atlas of Pre-Main-Sequence Stars. II. Far-Ultraviolet Accretion Diagnostics in T Tauri Stars. *ApJ* **2000**, *539*, 815–833. doi:10.1086/309259.
59. Calvet, N.; Hartmann, L.; Hewett, R.; Valenti, J.A.; Basri, G.; Walter, F. C IV in classical T Tauri stars. Cool Stars, Stellar Systems, and the Sun; Pallavicini, R.; Dupree, A.K., Eds., 1996, Vol. 109, *Astronomical Society of the Pacific Conference Series*, p. 419.
60. Valenti, J.A.; Basri, G.; Walter, F.; Hartmann, L.; Calvet, N. GHRS Profiles of Hot UV Lines in T Tauri Stars. American Astronomical Society Meeting Abstracts, 1993, Vol. 183, p. 40.07.
61. Yang, H.; Herczeg, G.J.; Linsky, J.L.; Brown, A.; Johns-Krull, C.M.; Ingleby, L.; Calvet, N.; Bergin, E.; Valenti, J.A. A Far-ultraviolet Atlas of Low-resolution Hubble Space Telescope Spectra of T Tauri Stars. *ApJ* **2012**, *744*, 121, [arXiv:astro-ph.SR/1205.4789]. doi:10.1088/0004-637X/744/2/121.
62. Muzerolle, J.; Calvet, N.; Hartmann, L. Magnetospheric Accretion Models for the Hydrogen Emission Lines of T Tauri Stars. *ApJ* **1998**, *492*, 743–753. doi:10.1086/305069.
63. Kwan, J.; Fischer, W. Origins of the H, He I and Ca II line emission in classical T Tauri stars. *MNRAS* **2011**, *411*, 2383–2425, [arXiv:astro-ph.SR/1010.3265]. doi:10.1111/j.1365-2966.2010.17863.x.
64. Ardila, D.R.; Herczeg, G.J.; Gregory, S.G.; Ingleby, L.; France, K.; Brown, A.; Edwards, S.; Johns-Krull, C.; Linsky, J.L.; Yang, H.; Valenti, J.A.; Abgrall, H.; Alexander, R.D.; Bergin, E.; Bethell, T.; Brown, J.M.; Calvet, N.; Espaillat, C.; Hillenbrand, L.A.; Hussain, G.; Roueff, E.; Schindhelm, E.R.; Walter, F.M. Hot Gas Lines in T Tauri Stars. *ApJs* **2013**, *207*, 1, [arXiv:astro-ph.SR/1304.3746]. doi:10.1088/0067-0049/207/1/1.

65. Lamzin, S.A. The structure of shock waves in the case of accretion onto low-mass young stars. *Astronomy Reports* **1998**, *42*, 322–335, [[arXiv:astro-ph.SR/1303.4066](#)].
66. Ardila, D.R.; Basri, G.; Walter, F.M.; Valenti, J.A.; Johns-Krull, C.M. Observations of T Tauri Stars using Hubble Space Telescope GHRS. I. Far-Ultraviolet Emission Lines. *ApJ* **2002**, *566*, 1100–1123, [[arXiv:astro-ph/astro-ph/0110436](#)]. doi:10.1086/338223.
67. Günther, H.M.; Schmitt, J.H.M.M. Where are the hot ion lines in classical T Tauri stars formed? *A&A* **2008**, *481*, 735–745, [[arXiv:astro-ph/0801.2273](#)]. doi:10.1051/0004-6361/20078674.
68. Herczeg, G.J.; Walter, F.M.; Linsky, J.L.; Gahm, G.F.; Ardila, D.R.; Brown, A.; Johns-Krull, C.M.; Simon, M.; Valenti, J.A. The Loopy Ultraviolet Line Profiles of RU Lupi: Accretion, Outflows, and Fluorescence. *AJ* **2005**, *129*, 2777–2791, [[arXiv:astro-ph/astro-ph/0504654](#)]. doi:10.1086/430075.
69. Lamzin, S.A. Intercombinational Line Profiles in the UV Spectra of T Tauri Stars and Analysis of the Accretion Zone. *Astronomy Reports* **2000**, *44*, 323–333. doi:10.1134/1.163855.
70. Ingleby, L.; Calvet, N.; Herczeg, G.; Blaty, A.; Walter, F.; Ardila, D.; Alexander, R.; Edwards, S.; Espaillat, C.; Gregory, S.G.; Hillenbrand, L.; Brown, A. Accretion Rates for T Tauri Stars Using Nearly Simultaneous Ultraviolet and Optical Spectra. *ApJ* **2013**, *767*, 112, [[arXiv:astro-ph.SR/1303.0769](#)]. doi:10.1088/0004-637X/767/2/112.
71. Robinson, C.E.; Espaillat, C.C. Multiepoch Ultraviolet HST Observations of Accreting Low-mass Stars. *ApJ* **2019**, *874*, 129, [[arXiv:astro-ph.SR/1903.01987](#)]. doi:10.3847/1538-4357/ab0d8d.
72. Gomez de Castro, A.I.; Lamzin, S.A. Accretion shocks in T Tauri stars: diagnosis via semiforbidden ultraviolet line ratios. *MNRAS* **1999**, *304*, L41–L45. doi:10.1046/j.1365-8711.1999.02545.x.
73. Matsakos, T.; Chièze, J.P.; Stehlé, C.; González, M.; Ibgui, L.; de Sá, L.; Lanz, T.; Orlando, S.; Bonito, R.; Argiroffi, C.; Reale, F.; Peres, G. YSO accretion shocks: magnetic, chromospheric or stochastic flow effects can suppress fluctuations of X-ray emission. *A&A* **2013**, *557*, A69, [[arXiv:astro-ph.SR/1307.5389](#)]. doi:10.1051/0004-6361/201321820.
74. Colombo, S.; Orlando, S.; Peres, G.; Argiroffi, C.; Reale, F. Impacts of fragmented accretion streams onto classical T Tauri stars: UV and X-ray emission lines. *A&A* **2016**, *594*, A93, [[arXiv:astro-ph.SR/1607.03009](#)]. doi:10.1051/0004-6361/201628858.
75. Schneider, P.C.; Günther, H.M.; Robrade, J.; Schmitt, J.H.M.M.; Güdel, M. Multiepoch, multiwavelength study of accretion onto T Tauri. X-ray versus optical and UV accretion tracers. *A&A* **2018**, *618*, A55, [[arXiv:astro-ph.SR/1806.06788](#)]. doi:10.1051/0004-6361/201731613.
76. Andrews, S.M.; Huang, J.; Pérez, L.M.; Isella, A.; Dullemond, C.P.; Kurtovic, N.T.; Guzmán, V.V.; Carpenter, J.M.; Wilner, D.J.; Zhang, S.; Zhu, Z.; Birnstiel, T.; Bai, X.N.; Benisty, M.; Hughes, A.M.; Öberg, K.I.; Ricci, L. ALMA Observations of the Epoch of Planet Formation. *The Messenger* **2018**, *174*, 19–23. doi:10.18727/0722-6691/5108.
77. Bary, J.S.; Weintraub, D.A.; Shukla, S.J.; Leisenring, J.M.; Kastner, J.H. Quiescent H₂ Emission From Pre-Main-Sequence Stars in Chamaeleon I. *ApJ* **2008**, *678*, 1088–1098, [[arXiv:astro-ph/0801.2765](#)]. doi:10.1086/529517.
78. Bitner, M.A.; Richter, M.J.; Lacy, J.H.; Herczeg, G.J.; Greathouse, T.K.; Jaffe, D.T.; Salyk, C.; Blake, G.A.; Hollenbach, D.J.; Doppmann, G.W.; Najita, J.R.; Currie, T. The TEXES Survey for H₂ Emission from Protoplanetary Disks. *ApJ* **2008**, *688*, 1326–1344, [[arXiv:astro-ph/0808.1099](#)]. doi:10.1086/592317.
79. Miotello, A.; Bruderer, S.; van Dishoeck, E.F. Protoplanetary disk masses from CO isotopologue line emission. *A&A* **2014**, *572*, A96, [[arXiv:astro-ph.SR/1410.2093](#)]. doi:10.1051/0004-6361/201424712.
80. Abgrall, H.; Roueff, E.; Launay, F.; Roncin, J.Y.; Subtil, J.L. Table of Lyman band system of molecular hydrogen. *A&As* **1993**, *101*, 273–321.
81. Abgrall, H.; Roueff, E.; Launay, F.; Roncin, J.Y.; Subtil, J.L. Table of the Werner band system of molecular hydrogen. *A&As* **1993**, *101*, 323–362.
82. Herczeg, G.J.; Wood, B.E.; Linsky, J.L.; Valenti, J.A.; Johns-Krull, C.M. The Far-Ultraviolet Spectra of TW Hydrae. II. Models of H₂ Fluorescence in a Disk. *ApJ* **2004**, *607*, 369–383, [[arXiv:astro-ph/astro-ph/0402238](#)]. doi:10.1086/383340.

83. France, K.; Schindhelm, E.; Herczeg, G.J.; Brown, A.; Abgrall, H.; Alexander, R.D.; Bergin, E.A.; Brown, J.M.; Linsky, J.L.; Roueff, E.; Yang, H. A Hubble Space Telescope Survey of H₂ Emission in the Circumstellar Environments of Young Stars. *ApJ* **2012**, *756*, 171, [arXiv:astro-ph.SR/1207.4789]. doi:10.1088/0004-637X/756/2/171.
84. Hoadley, K.; France, K.; Alexander, R.D.; McJunkin, M.; Schneider, P.C. The Evolution of Inner Disk Gas in Transition Disks. *ApJ* **2015**, *812*, 41, [arXiv:astro-ph.SR/1509.02172]. doi:10.1088/0004-637X/812/1/41.
85. Ádámkóvics, M.; Najita, J.R.; Glassgold, A.E. FUV Irradiated Disk Atmospheres: Ly α and the Origin of Hot H₂ Emission. *ApJ* **2016**, *817*, 82, [arXiv:astro-ph.SR/1512.04425]. doi:10.3847/0004-637X/817/1/82.
86. France, K.; Beasley, M.; Ardila, D.R.; Bergin, E.A.; Brown, A.; Burgh, E.B.; Calvet, N.; Chiang, E.; Cook, T.A.; Désert, J.M.; Ebbets, D.; Froning, C.S.; Green, J.C.; Hillenbrand, L.A.; Johns-Krull, C.M.; Koskinen, T.T.; Linsky, J.L.; Redfield, S.; Roberge, A.; Schindhelm, E.R.; Scowen, P.A.; Stapelfeldt, K.R.; Tumlison, J. From Protoplanetary Disks to Extrasolar Planets: Understanding the Life Cycle of Circumstellar Gas with Ultraviolet Spectroscopy. *arXiv e-prints* **2012**, p. arXiv:1208.2270, [arXiv:astro-ph.SR/1208.2270].
87. France, K.; Burgh, E.B.; Herczeg, G.J.; Schindhelm, E.; Yang, H.; Abgrall, H.; Roueff, E.; Brown, A.; Brown, J.M.; Linsky, J.L. CO and H₂ Absorption in the AA Tauri Circumstellar Disk. *ApJ* **2012**, *744*, 22, [arXiv:astro-ph.SR/1109.1831]. doi:10.1088/0004-637X/744/1/22.
88. Hoadley, K.; France, K.; Arulanantham, N.; Loyd, R.O.P.; Kruczek, N. Signatures of Hot Molecular Hydrogen Absorption from Protoplanetary Disks. I. Non-thermal Populations. *ApJ* **2017**, *846*, 6, [arXiv:astro-ph.SR/1707.03449]. doi:10.3847/1538-4357/aa7fc1.
89. Schneider, P.C.; France, K.; Günther, H.M.; Herczeg, G.; Robrade, J.; Bouvier, J.; McJunkin, M.; Schmitt, J.H.M.M. X-ray to NIR emission from AA Tauri during the dim state. Occultation of the inner disk and gas-to-dust ratio of the absorber. *A&A* **2015**, *584*, A51, [arXiv:astro-ph.SR/1509.05007]. doi:10.1051/0004-6361/201425583.
90. Herczeg, G.J.; Linsky, J.L.; Walter, F.M.; Gahm, G.F.; Johns-Krull, C.M. The Origins of Fluorescent H₂ Emission From T Tauri Stars. *ApJs* **2006**, *165*, 256–282, [arXiv:astro-ph/astro-ph/0602404]. doi:10.1086/503558.
91. Salyk, C.; Blake, G.A.; Boogert, A.C.A.; Brown, J.M. High-resolution 5 μ m Spectroscopy of Transitional Disks. *ApJ* **2009**, *699*, 330–347. doi:10.1088/0004-637X/699/1/330.
92. Salyk, C.; Blake, G.A.; Boogert, A.C.A.; Brown, J.M. CO Rovibrational Emission as a Probe of Inner Disk Structure. *ApJ* **2011**, *743*, 112, [arXiv:astro-ph.GA/1109.4579]. doi:10.1088/0004-637X/743/2/112.
93. Brown, J.M.; Pontoppidan, K.M.; van Dishoeck, E.F.; Herczeg, G.J.; Blake, G.A.; Smette, A. VLT-CRIRES Survey of Rovibrational CO Emission from Protoplanetary Disks. *ApJ* **2013**, *770*, 94, [arXiv:astro-ph.SR/1304.4961]. doi:10.1088/0004-637X/770/2/94.
94. Bergin, E.; Calvet, N.; D’Alessio, P.; Herczeg, G.J. The Effects of UV Continuum and Ly α Radiation on the Chemical Equilibrium of T Tauri Disks. *ApJl* **2003**, *591*, L159–L162, [arXiv:astro-ph/astro-ph/0305565]. doi:10.1086/377148.
95. Ingleby, L.; Calvet, N.; Bergin, E.; Yerasi, A.; Espaillat, C.; Herczeg, G.; Roueff, E.; Abgrall, H.; Hernández, J.; Briceño, C.; Pascucci, I.; Miller, J.; Fogel, J.; Hartmann, L.; Meyer, M.; Carpenter, J.; Crockett, N.; McClure, M. Far-Ultraviolet H₂ Emission from Circumstellar Disks. *ApJl* **2009**, *703*, L137–L141, [arXiv:astro-ph.SR/0909.0688]. doi:10.1088/0004-637X/703/2/L137.
96. Espaillat, C.C.; Robinson, C.; Grant, S.; Reynolds, M. Using Multiwavelength Variability to Explore the Connection among X-Ray Emission, the Far-ultraviolet H₂ Bump, and Accretion in T Tauri Stars. *ApJ* **2019**, *876*, 121, [arXiv:astro-ph.SR/1904.05458]. doi:10.3847/1538-4357/ab16e6.
97. Burgh, E.B.; France, K.; McCandliss, S.R. Direct Measurement of the Ratio of Carbon Monoxide to Molecular Hydrogen in the Diffuse Interstellar Medium. *ApJ* **2007**, *658*, 446–454, [arXiv:astro-ph/astro-ph/0611853]. doi:10.1086/511259.
98. Feldman, P.D.; Burgh, E.B.; Durrance, S.T.; Davidsen, A.F. Far-Ultraviolet Spectroscopy of Venus and Mars at 4 Å Resolution with the Hopkins Ultraviolet Telescope on Astro-2. *ApJ* **2000**, *538*, 395–400, [arXiv:astro-ph/astro-ph/0004024]. doi:10.1086/309125.

99. McJunkin, M.; France, K.; Burgh, E.B.; Herczeg, G.J.; Schindhelm, E.; Brown, J.M.; Brown, A. Probing the Inner Regions of Protoplanetary Disks with CO Absorption Line Spectroscopy. *ApJ* **2013**, *766*, 12, [[arXiv:astro-ph.SR/1302.0738](#)]. doi:10.1088/0004-637X/766/1/12.
100. Woitke, P.; Riaz, B.; Duchêne, G.; Pascucci, I.; Lyo, A.R.; Dent, W.R.F.; Phillips, N.; Thi, W.F.; Ménard, F.; Herczeg, G.J.; Bergin, E.; Brown, A.; Mora, A.; Kamp, I.; Aresu, G.; Brittain, S.; de Gregorio-Monsalvo, I.; Sandell, G. The unusual protoplanetary disk around the T Tauri star ET Chamaeleontis. *A&A* **2011**, *534*, A44, [[arXiv:astro-ph.EP/1103.5309](#)]. doi:10.1051/0004-6361/201116684.
101. France, K.; Schindhelm, E.; Bergin, E.A.; Roueff, E.; Abgrall, H. High-resolution Ultraviolet Radiation Fields of Classical T Tauri Stars. *ApJ* **2014**, *784*, 127, [[arXiv:astro-ph.SR/1402.6341](#)]. doi:10.1088/0004-637X/784/2/127.
102. France, K.; Fleming, B.; West, G.; McCandliss, S.R.; Bolcar, M.R.; Harris, W.; Moustakas, L.; O'Meara, J.M.; Pascucci, I.; Rigby, J.; Schiminovich, D.; Tumlinson, J. The LUVUOIR Ultraviolet Multi-Object Spectrograph (LUMOS): instrument definition and design. *SPIE Proceedings*, 2017, Vol. 10397, *Society of Photo-Optical Instrumentation Engineers (SPIE) Conference Series*, p. 1039713, [[arXiv:astro-ph.IM/1709.06141](#)]. doi:10.1117/12.2272025.
103. Walsh, C.; Nomura, H.; Millar, T.J.; Aikawa, Y. Chemical Processes in Protoplanetary Disks. II. On the Importance of Photochemistry and X-Ray Ionization. *ApJ* **2012**, *747*, 114, [[arXiv:astro-ph.GA/1201.2613](#)]. doi:10.1088/0004-637X/747/2/114.
104. Bergin, E.A.; Aikawa, Y.; Blake, G.A.; van Dishoeck, E.F. The Chemical Evolution of Protoplanetary Disks. *Protostars and Planets V*; Reipurth, B.; Jewitt, D.; Keil, K., Eds., 2007, p. 751, [[arXiv:astro-ph/astro-ph/0603358](#)].
105. Shull, J.M.; Beckwith, S. Interstellar molecular hydrogen. *ARA&A* **1982**, *20*, 163–190. doi:10.1146/annurev.aa.20.090182.001115.
106. van Dishoeck, E.F.; Black, J.H. The Photodissociation and Chemistry of Interstellar CO. *ApJ* **1988**, *334*, 771. doi:10.1086/166877.
107. van Zadelhoff, G.J.; Aikawa, Y.; Hogerheijde, M.R.; van Dishoeck, E.F. Axis-symmetric models of ultraviolet radiative transfer with applications to circumstellar disk chemistry. *A&A* **2003**, *397*, 789–802, [[arXiv:astro-ph/astro-ph/0211014](#)]. doi:10.1051/0004-6361:20021592.
108. Vasyunin, A.I.; Wiebe, D.S.; Birnstiel, T.; Zhukovska, S.; Henning, T.; Dullemond, C.P. Impact of Grain Evolution on the Chemical Structure of Protoplanetary Disks. *ApJ* **2011**, *727*, 76, [[arXiv:astro-ph.GA/1011.4420](#)]. doi:10.1088/0004-637X/727/2/76.
109. Bethell, T.J.; Bergin, E.A. The Propagation of Ly α in Evolving Protoplanetary Disks. *ApJ* **2011**, *739*, 78, [[arXiv:astro-ph.SR/1107.3514](#)]. doi:10.1088/0004-637X/739/2/78.
110. Fogel, J.K.J.; Bethell, T.J.; Bergin, E.A.; Calvet, N.; Semenov, D. Chemistry of a Protoplanetary Disk with Grain Settling and Ly α Radiation. *ApJ* **2011**, *726*, 29, [[arXiv:astro-ph.SR/1011.0446](#)]. doi:10.1088/0004-637X/726/1/29.
111. McJunkin, M.; France, K.; Schindhelm, E.; Herczeg, G.; Schneider, P.C.; Brown, A. Empirically Estimated Far-UV Extinction Curves for Classical T Tauri Stars. *ApJ* **2016**, *828*, 69. doi:10.3847/0004-637X/828/2/69.
112. Fedele, D.; van den Ancker, M.E.; Henning, T.; Jayawardhana, R.; Oliveira, J.M. Timescale of mass accretion in pre-main-sequence stars. *A&A* **2010**, *510*, A72, [[arXiv:astro-ph.SR/0911.3320](#)]. doi:10.1051/0004-6361/200912810.
113. Alexander, R.D.; Clarke, C.J.; Pringle, J.E. Photoevaporation of protoplanetary discs - I. Hydrodynamic models. *MNRAS* **2006**, *369*, 216–228, [[arXiv:astro-ph/astro-ph/0603253](#)]. doi:10.1111/j.1365-2966.2006.10293.x.
114. Gorti, U.; Hollenbach, D. Photoevaporation of Circumstellar Disks By Far-Ultraviolet, Extreme-Ultraviolet and X-Ray Radiation from the Central Star. *ApJ* **2009**, *690*, 1539–1552, [[arXiv:astro-ph/0809.1494](#)]. doi:10.1088/0004-637X/690/2/1539.
115. Dodson-Robinson, S.E.; Salyk, C. Transitional Disks as Signposts of Young, Multiplanet Systems. *ApJ* **2011**, *738*, 131, [[arXiv:astro-ph.EP/1106.4824](#)]. doi:10.1088/0004-637X/738/2/131.
116. Chiang, E.; Murray-Clay, R. Inside-out evacuation of transitional protoplanetary discs by the magneto-rotational instability. *Nature Physics* **2007**, *3*, 604–608, [[arXiv:astro-ph/0706.1241](#)]. doi:10.1038/nphys661.

117. Banzatti, A.; Pontoppidan, K.M. An Empirical Sequence of Disk Gap Opening Revealed by Rovibrational CO. *ApJ* **2015**, *809*, 167, [arXiv:astro-ph.EP/1507.06650]. doi:10.1088/0004-637X/809/2/167.
118. Arulanantham, N.; France, K.; Hoadley, K.; Manara, C.F.; Schneider, P.C.; Alcalá, J.M.; Banzatti, A.; Günther, H.M.; Miotello, A.; van der Marel, N.; van Dishoeck, E.F.; Walsh, C.; Williams, J.P. A UV-to-NIR Study of Molecular Gas in the Dust Cavity around RY Lupi. *ApJ* **2018**, *855*, 98, [arXiv:astro-ph.SR/1802.05275]. doi:10.3847/1538-4357/aaaf65.
119. Frank, A.; Ray, T.P.; Cabrit, S.; Hartigan, P.; Arce, H.G.; Bacciotti, F.; Bally, J.; Benisty, M.; Eisloffel, J.; Güdel, M.; Lebedev, S.; Nisini, B.; Raga, A. Jets and Outflows from Star to Cloud: Observations Confront Theory. Protostars and Planets VI; Beuther, H.; Klessen, R.S.; Dullemond, C.P.; Henning, T., Eds., 2014, p. 451, [arXiv:astro-ph.SR/1402.3553]. doi:10.2458/azu_uapress_9780816531240-ch020.
120. Zanni, C.; Ferreira, J. MHD simulations of accretion onto a dipolar magnetosphere. II. Magnetospheric ejections and stellar spin-down. *A&A* **2013**, *550*, A99, [arXiv:astro-ph.SR/1211.4844]. doi:10.1051/0004-6361/201220168.
121. Shu, F.; Najita, J.; Ostriker, E.; Wilkin, F.; Ruden, S.; Lizano, S. Magnetocentrifugally Driven Flows from Young Stars and Disks. I. A Generalized Model. *ApJ* **1994**, *429*, 781. doi:10.1086/174363.
122. Blandford, R.D.; Payne, D.G. Hydromagnetic flows from accretion disks and the production of radio jets. *MNRAS* **1982**, *199*, 883–903. doi:10.1093/mnras/199.4.883.
123. Raga, A.C.; Reipurth, B.; Castellanos-Ramírez, A.; Chiang, H.F.; Bally, J. Collisionally Excited Filaments in Hubble Space Telescope H α and H β Images of HH 1/2. *ApJl* **2015**, *798*, L1, [arXiv:astro-ph.SR/1411.7972]. doi:10.1088/2041-8205/798/1/L1.
124. Loinard, L.; Zapata, L.A.; Rodriguez, L.F.; Pech, G.; Chandler, C.J.; Brogan, C.L.; Wilner, D.J.; Ho, P.T.P.; Parise, B.; Hartmann, L.W.; Zhu, Z.; Takahashi, S.; Trejo, A. ALMA and VLA observations of the outflows in IRAS 16293-2422. *MNRAS* **2013**, *430*, L10–L14, [arXiv:astro-ph.SR/1211.4744]. doi:10.1093/mnrasl/sls038.
125. Güdel, M.; Eibensteiner, C.; Dionatos, O.; Audard, M.; Forbrich, J.; Kraus, S.; Rab, C.; Schneider, C.; Skinner, S.; Vorobyov, E. ALMA detects a radial disk wind in DG Tauri. *A&A* **2018**, *620*, L1, [arXiv:astro-ph.SR/1810.12251]. doi:10.1051/0004-6361/201834271.
126. Pravdo, S.H.; Feigelson, E.D.; Garmire, G.; Maeda, Y.; Tsuboi, Y.; Bally, J. Discovery of X-rays from the protostellar outflow object HH2. *Nature* **2001**, *413*, 708–711. doi:10.1038/35099508.
127. Güdel, M.; Skinner, S.L.; Audard, M.; Briggs, K.R.; Cabrit, S. Discovery of a bipolar X-ray jet from the T Tauri star DG Tauri. *A&A* **2008**, *478*, 797–807, [arXiv:astro-ph/0712.1330]. doi:10.1051/0004-6361:20078141.
128. Schneider, P.C.; Günther, H.M.; Schmitt, J.H.M.M. The X-ray puzzle of the L1551 IRS 5 jet. *A&A* **2011**, *530*, A123, [arXiv:astro-ph.SR/1105.1663]. doi:10.1051/0004-6361/201016305.
129. Ainsworth, R.E.; Scaife, A.M.M.; Ray, T.P.; Taylor, A.M.; Green, D.A.; Buckle, J.V. Tentative Evidence for Relativistic Electrons Generated by the Jet of the Young Sun-like Star DG Tau. *ApJl* **2014**, *792*, L18, [arXiv:astro-ph.SR/1408.1892]. doi:10.1088/2041-8205/792/1/L18.
130. Dupree, A.K.; Brickhouse, N.S.; Smith, G.H.; Strader, J. A Hot Wind from the Classical T Tauri Stars: TW Hydrae and T Tauri. *ApJl* **2005**, *625*, L131–L134, [arXiv:astro-ph/astro-ph/0505037]. doi:10.1086/431323.
131. Skinner, S.L.; Schneider, P.C.; Audard, M.; Güdel, M. Resolving the Inner Arcsecond of the RY Tau Jet with HST. *ApJ* **2018**, *855*, 143, [arXiv:astro-ph.SR/1801.08568]. doi:10.3847/1538-4357/aaab58.
132. Schneider, P.C.; Schmitt, J.H.M.M. The nature of the soft X-ray source in DG Tauri. *A&A* **2008**, *488*, L13–L16, [arXiv:astro-ph/0807.2156]. doi:10.1051/0004-6361:200810261.
133. Walter, F.M.; Herczeg, G.; Brown, A.; Ardila, D.R.; Gahm, G.F.; Johns-Krull, C.M.; Lissauer, J.J.; Simon, M.; Valenti, J.A. Mapping the Circumstellar Environment of T Tauri with Fluorescent H₂ Emission. *AJ* **2003**, *126*, 3076–3089, [arXiv:astro-ph/astro-ph/0309142]. doi:10.1086/379557.
134. Schneider, P.C.; Eisloffel, J.; Güdel, M.; Günther, H.M.; Herczeg, G.; Robrade, J.; Schmitt, J.H.M.M. HST far-ultraviolet imaging of DG Tauri. Fluorescent molecular hydrogen emission from the wide opening-angle outflow. *A&A* **2013**, *557*, A110, [arXiv:astro-ph.SR/1307.2846]. doi:10.1051/0004-6361/201321564.
135. Agra-Amboage, V.; Cabrit, S.; Dougados, C.; Kristensen, L.E.; Ibgui, L.; Reunanen, J. Origin of the wide-angle hot H₂ in DG Tauri. New insight from SINFONI spectro-imaging. *A&A* **2014**, *564*, A11, [arXiv:astro-ph.SR/1402.1160]. doi:10.1051/0004-6361/201220488.

136. Costigan, G.; Vink, J.S.; Scholz, A.; Ray, T.; Testi, L. Temperaments of young stars: rapid mass accretion rate changes in T Tauri and Herbig Ae stars. *MNRAS* **2014**, *440*, 3444–3461, [[arXiv:astro-ph.SR/1403.4088](#)]. doi:10.1093/mnras/stu529.
137. Gómez de Castro, A.I.; Fernández, M. Ultraviolet spectroscopy of the hotspot in the classical T Tauri star DI Cep: observational indications of magnetically channelled accretion. *MNRAS* **1996**, *283*, 55–65. doi:10.1093/mnras/283.1.55.
138. Gómez de Castro, A.I.; Franqueira, M. Accretion and UV Variability in BP Tauri. *ApJ* **1997**, *482*, 465–469. doi:10.1086/304149.
139. Ismailov, N.Z.; Alimardanova, F.N.; Baheddinova, G.R.; Adygezalade, H.N. Ultraviolet Spectrum Variability of BP Tau. *Odessa Astronomical Publications* **2010**, *23*, 46.
140. Ingleby, L.; Espaillat, C.; Calvet, N.; Sitko, M.; Russell, R.; Champney, E. Using FUV to IR Variability to Probe the Star-Disk Connection in the Transitional Disk of GM Aur. *ApJ* **2015**, *805*, 149, [[arXiv:astro-ph.SR/1504.00562](#)]. doi:10.1088/0004-637X/805/2/149.
141. Lamzin, S.A.; Kravtsova, A.S.; Romanova, M.M.; Batalha, C. Kinematics and Parameters of the Gas in the Vicinity of TW Hya. *Astronomy Letters* **2004**, *30*, 413–427. doi:10.1134/1.1764888.
142. Kastner, J.H.; Huenemoerder, D.P.; Schulz, N.S.; Canizares, C.R.; Weintraub, D.A. Evidence for Accretion: High-Resolution X-Ray Spectroscopy of the Classical T Tauri Star TW Hydrae. *ApJ* **2002**, *567*, 434–440, [[arXiv:astro-ph/astro-ph/0111049](#)]. doi:10.1086/338419.
143. Brickhouse, N.S.; Cranmer, S.R.; Dupree, A.K.; Luna, G.J.M.; Wolk, S. A Deep Chandra X-Ray Spectrum of the Accreting Young Star TW Hydrae. *ApJ* **2010**, *710*, 1835–1847, [[arXiv:astro-ph.SR/1001.0750](#)]. doi:10.1088/0004-637X/710/2/1835.
144. Curran, R.L.; Argiroffi, C.; Sacco, G.G.; Orland o, S.; Peres, G.; Reale, F.; Maggio, A. Multiwavelength diagnostics of accretion in an X-ray selected sample of CTTs. *A&A* **2011**, *526*, A104, [[arXiv:astro-ph.SR/1011.5915](#)]. doi:10.1051/0004-6361/201015522.
145. Günther, H.M.; Schmitt, J.H.M.M.; Robrade, J.; Liefke, C. X-ray emission from classical T Tauri stars: accretion shocks and coronae? *A&A* **2007**, *466*, 1111–1121, [[arXiv:astro-ph/astro-ph/0702579](#)]. doi:10.1051/0004-6361:20065669.
146. Bouvier, J.; Grankin, K.; Ellerbroek, L.E.; Bouy, H.; Barrado, D. AA Tauri’s sudden and long-lasting deepening: enhanced extinction by its circumstellar disk. *A&A* **2013**, *557*, A77, [[arXiv:astro-ph.SR/1304.1487](#)]. doi:10.1051/0004-6361/201321389.
147. Reipurth, B.; Aspin, C. FUors and Early Stellar Evolution. Evolution of Cosmic Objects through their Physical Activity; Harutyunian, H.A.; Mickaelian, A.M.; Terzian, Y., Eds., 2010, pp. 19–38.
148. Kenyon, S.J.; Hartmann, L.; Imhoff, C.L.; Cassatella, A. Ultraviolet Spectroscopy of Pre–Main-Sequence Accretion Disks. *ApJ* **1989**, *344*, 925. doi:10.1086/167860.
149. Kravtsova, A.S.; Lamzin, S.A.; Errico, L.; Vittone, A. Ultraviolet spectrum of FU Ori and a “Compromise” model of the FUor. *Astronomy Letters* **2007**, *33*, 755–765. doi:10.1134/S1063773707110060.
150. Devine, D.; Grady, C.A.; Kimble, R.A.; Woodgate, B.; Bruhweiler, F.C.; Boggess, A.; Linsky, J.L.; Clampin, M. A Ly α Bright Jet from a Herbig AE Star. *ApJ* **2000**, *542*, L115–L118. doi:10.1086/312939.
151. Günther, H.M.; Schneider, P.C.; Li, Z.Y. The evolution of the jet from Herbig Ae star HD 163296 from 1999 to 2011. *A&A* **2013**, *552*, A142, [[arXiv:astro-ph.SR/1302.3233](#)]. doi:10.1051/0004-6361/201220772.
152. Rodríguez, L.F.; González, R.F.; Raga, A.C.; Cantó, J.; Riera, A.; Loinard, L.; Dzib, S.A.; Zapata, L.A. Radio continuum emission from knots in the DG Tauri jet. *A&A* **2012**, *537*, A123, [[arXiv:astro-ph.GA/1111.1196](#)]. doi:10.1051/0004-6361/201117991.
153. France, K.; Fleming, B.; West, G.; McCand liss, S.R.; Bolcar, M.R.; Harris, W.; Moustakas, L.; O’Meara, J.M.; Pascucci, I.; Rigby, J.; Schiminovich, D.; Tumlinson, J. The LUVOR Ultraviolet Multi-Object Spectrograph (LUMOS): instrument definition and design. SPIE Proceedings, 2017, Vol. 10397, *Society of Photo-Optical Instrumentation Engineers (SPIE) Conference Series*, p. 1039713, [[arXiv:astro-ph.IM/1709.06141](#)]. doi:10.1117/12.2272025.

154. The LUVOIR Team. The LUVOIR Mission Concept Study Interim Report. *arXiv e-prints* 2018, p. arXiv:1809.09668, [[arXiv:astro-ph.IM/1809.09668](https://arxiv.org/abs/astro-ph.IM/1809.09668)].



© 2019 by the authors. Licensee MDPI, Basel, Switzerland. This article is an open access article distributed under the terms and conditions of the Creative Commons Attribution (CC BY) license (<http://creativecommons.org/licenses/by/4.0/>).